

AD-754 915

FINITE ELEMENT MODELING AND OPTIMIZA-
TION OF AEROSPACE STRUCTURES

Walter J. Dwyer

Grumman Aerospace Corporation

Prepared for:

Air Force Flight Dynamics Laboratory

August 1972

DISTRIBUTED BY:

NTIS

National Technical Information Service
U. S. DEPARTMENT OF COMMERCE
5285 Port Royal Road, Springfield Va. 22151

AFFDL-TR-72-59

AD 754915

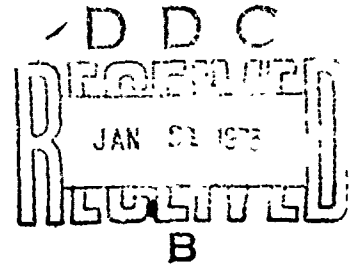
FINITE ELEMENT MODELING AND OPTIMIZATION OF AEROSPACE STRUCTURES

WALTER J. DWYER

GRUMMAN AEROSPACE CORPORATION

TECHNICAL REPORT AFFDL-TR-72-59

AUGUST 1972



This document has been approved for public release
and sale; its distribution is unlimited.

Reproduced by
NATIONAL TECHNICAL
INFORMATION SERVICE
U S Department of Commerce
Springfield VA 22151

AIR FORCE FLIGHT DYNAMICS LABORATORY
AIR FORCE SYSTEMS COMMAND
WRIGHT-PATTERSON AIR FORCE BASE, OHIO

NOTICE

When Government drawings, specifications, or other data are used for any purpose other than in connection with a definitely related Government procurement operation, the United States Government thereby incurs no responsibility nor any obligation whatsoever; and the fact that the government may have formulated, furnished, or in any way supplied the said drawings, specifications, or other data, is not to be regarded by implication or otherwise as in any manner licensing the holder or any other person or corporation, or conveying any rights or permission to manufacture, use, or sell any patented invention that may in any way be related thereto.

ACCESSION for		
NTIS	White Section	<input checked="" type="checkbox"/>
C C	Dev. Section	<input type="checkbox"/>
UNCLASSIFIED		<input type="checkbox"/>
BY		
DISTRIBUTION/AVAILABILITY CODES		
DIST.	AVAIL.	SPECIAL
A		

Copies of this report should not be returned unless return is required by security considerations, contractual obligations, or notice on a specific document.

Unclassified

Security Classification

14 KEY WORDS	LINK A		LINK B		LINK C	
	ROLE	WT	ROLE	WT	ROLE	WT
Finite Element Method Structural Optimization Automated Design						

Unclassified

Security Classification

Unclassified

Security Classification

DOCUMENT CONTROL DATA - R & D		
<i>(Security classification of title, body of abstract and indexing annotation must be entered when the overall report is classified)</i>		
1. ORIGINATING ACTIVITY (Corporate author)	2a. REPORT SECURITY CLASSIFICATION	
Grumman Aerospace Corporation Bethpage, New York	Unclassified	
	2b. GROUP	
3. REPORT TITLE		
Finite Element Modeling and Optimization of Aerospace Structures		
4. DESCRIPTIVE NOTES (Type of report and inclusive dates)		
Final		
5. AUTHOR(S) (First name, middle initial, last name)		
Walter J. Dwyer		
6. REPORT DATE	7a. TOTAL NO. OF PAGES	7b. NO. OF REFS
August 1972	50 59	3
8a. CONTRACT OR GRANT NO.	9a. ORIGINATOR'S REPORT NUMBER(S)	
F33615-72-C-1466	AFFDL TR-72-59	
b. PROJECT NO.		
c.	9b. OTHER REPORT NO(S) (Any other numbers that may be assigned this report)	
d.		
10. DISTRIBUTION STATEMENT		
Distribution of this document is unlimited.		
11. SUPPLEMENTARY NOTES	12. SPONSORING MILITARY ACTIVITY	
	Air Force Flight Dynamics Laboratory Wright-Patterson AFB, Ohio	
13. ABSTRACT		
<p>This report documents a study made of the optimization of typical aircraft structural components using the Automated Structural Optimization Program (ASOP) described in AFFDL-TR-70-118. The structures examined were a fuselage structure for a proposed space shuttle orbiter and a wing structure for the same vehicle. Examples are given of practical finite element modeling of these structures. (U)</p>		

DD FORM 1 NOV 65 1473

Unclassified

Security Classification

AFFDL-TR-72-59

**FINITE ELEMENT MODELING AND
OPTIMIZATION OF AEROSPACE STRUCTURES**

WALTER J. DWYER

GRUMMAN AEROSPACE CORPORATION

TECHNICAL REPORT AFFDL-TR-72-59

AUGUST 1972

This document has been approved for public release
and sale; its distribution is unlimited.

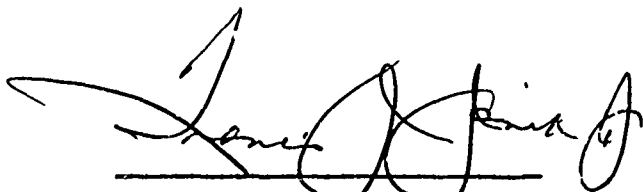
AIR FORCE FLIGHT DYNAMICS LABORATORY
AIR FORCE SYSTEMS COMMAND
WRIGHT-PATTERSON AIR FORCE BASE, OHIO

FOREWORD

This report was prepared by the Structural Mechanics Section of the Grumman Aerospace Corporation, Bethpage, New York. It documents work done under USAF Contract F33615-71-C-1466, which was initiated under Project No. 1467, "Structural Optimization Methods For Aerospace Vehicles," Task No. 146701. The effort was administered by the Air Force Flight Dynamics Laboratory, Air Force Systems Command, Wright Patterson Air Force Base, Ohio. Dr. Vipperla B. Venkayya (AFFDL/FBR) was the Project Monitor. The Project Engineer and Principal Investigator of the present effort was Dr. Walter J. Dwyer, Structural Methods Engineer, Structural Mechanics Section.

This report covers work from 15 April 1971 to 15 April 1972 and was submitted to the Air Force in April 1972.

The technical report has been reviewed and is approved.



Francis J. Janik, Jr.
Chief Theoretical Mechanics Branch
Air Force Flight Dynamics Laboratory

TABLE OF CONTENTS

	<u>PAGE</u>
INTRODUCTION	1
DISCUSSION	4
A Wing Design Study	4
1. Structural Idealization	4
2. Loading Conditions	8
3. Design Criteria	11
4. Optimization Results	13
B Fuselage Design Study	15
1. Structural Idealization	15
2. Loading Conditions	30
3. Design Criteria	37
4. Optimization Results	38
REFERENCES	45
APPENDIX A	46
APPENDIX B	47

List of Figures	Page
1. General Structural Arrangement of the H-3T Orbiter	3
2. Idealization of Orbiter Wing	5
3. Portion of Typical Wing Cross Section	6
4. Finite Element Idealization of Typical Cover Element	8
5. Ultimate Loads Per Side Acting on the Orbiter Wing	9
6. Distribution of Applied Loads on the Orbiter Wing	10
7. Conventional Cover Allowable Compressive Stress	12
8. Thicknesses of Optimized Orbiter Wing Top Cover Elements	14
9. Left Half of Orbiter Fuselage Finite Element Model	16
10. Fuselage Bulkhead Idealizations	20
11. Fuselage Bulkhead Structural Arrangements	24
12. Mission Profile	31
13. H-3T Orbiter Applied Loading Conditions	32
14. Summary of Applied Loading Conditions	33
15. H-3T Orbiter Fuselage Ultimate Bending Moment Envelope	34
16. H-3T Orbiter Fuselage Ultimate Vertical Shear Envelope	35
17. H-3T Orbiter Fuselage Ultimate Axial Load Envelope	36
18. Modulus Ratio for Buckled Elastic Web	37
19. Allowable Compressive Stress for Bar Elements	39
20. Main Longerons of H-3T Orbiter Fuselage, Left Half	41
21. Areas and Critical Loading Conditions for the H-3T Main Longerons Starting from Hand Calculated Sizes	42
22. Areas for the H-3T Main Longerons After Optimization Starting with Uniform Sizes	43
23. Integrally Stiffened Panel	47
24. Appendix 8	48

INTRODUCTION

Automated structural optimization methods using finite-element analysis are now available with sufficient capability to be used in practical design studies. To examine their use in an actual design, the optimization of two components of a shuttle orbiter vehicle is described. The computer program used is the Automated Structural Optimization Program (ASOP) described in Reference 1. Several extensions of this program which were developed to increase its generality are also described.

Many different orbiter and booster configurations were examined during Grumman's initial studies of the space shuttle system. In these studies the ASOP program was used extensively on the wing and tail surfaces. However, because of the lack of experience with the optimization of fuselage structures, no automated optimization of the fuselage was initially attempted. For the study reported herein, use of the program for optimization of both the wing and the fuselage was undertaken to demonstrate the versatility of ASOP. Results obtained from the automated design procedure are compared with the structural design obtained by more traditional methods.

The particular design chosen for this study is known as the H-3T configuration; its general structural arrangement is shown in Figure 1. The orbiter vehicle for this design has a delta wing and two main propulsion engines. Four air breathing engines are also provided for flight within the atmosphere. The liquid hydrogen for the main propulsion engines is carried in two external disposable tanks attached to the side of the fuselage. The crew compartment is also jettisonable in an emergency and is not structurally

part of the fuselage. Access to the payload is through clam shell doors along the top of the fuselage. These doors are also not part of the primary structure.

This report shows how both the wing and fuselage structures are idealized into finite element mathematical models. This will serve to guide the program user in establishing the idealizations needed for the optimization process. To demonstrate the program's usefulness, results obtained from the automated calculations for the element gages are compared to material distributions obtained by the more traditional non-automated methods. To demonstrate the program's convergence characteristics, the fuselage structure was optimized twice starting with different material distributions, with essentially the same final results.

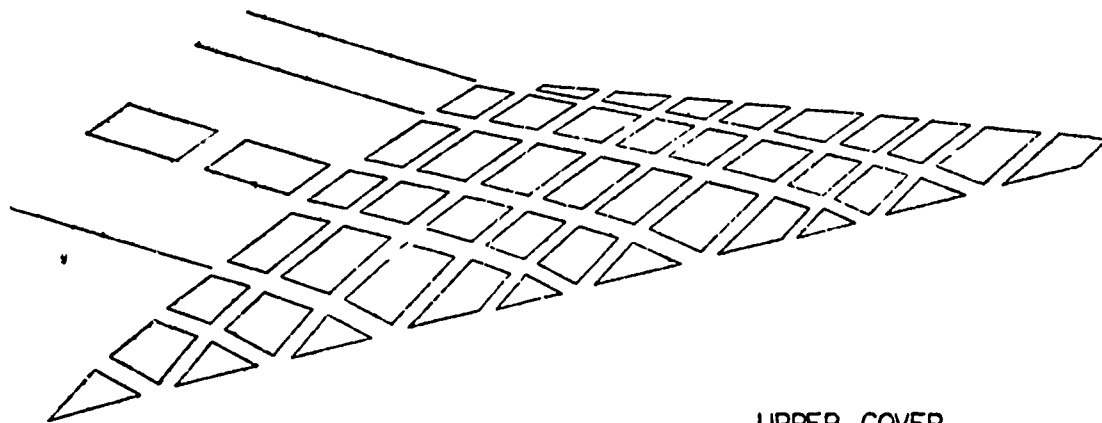
DISCUSSION

A. Wing Design Study

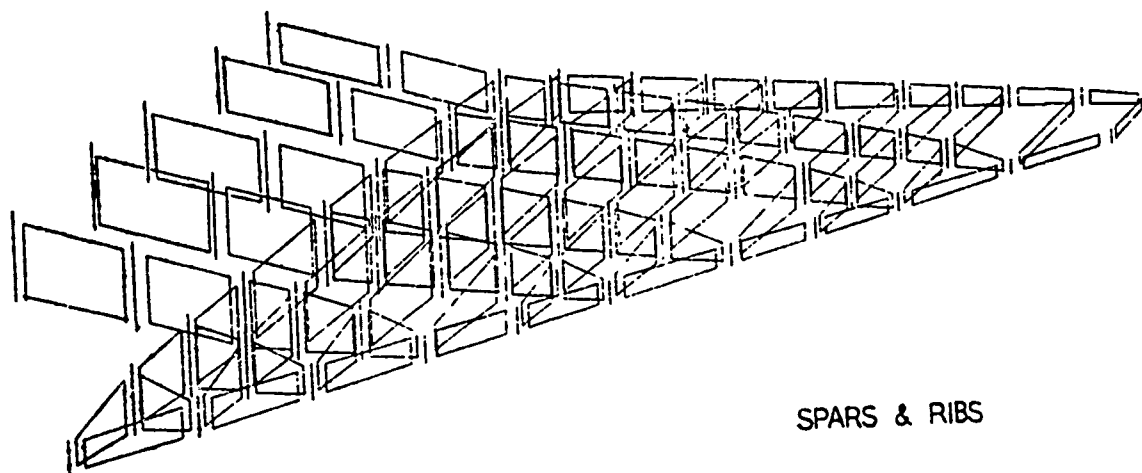
1. Structural Idealization

The general planform of the wing is shown in Figure 1. The semi-span from the centerline of the fuselage to the tip is about 650 inches; the root chord is approximately 800 inches. The development of the finite-element model of the primary structural box evolves naturally from the defined positions of the spars and ribs as shown in Figure 2. Each of the covers, outboard of the root, is idealized as anisotropic membrane quadrilateral and triangular elements which carry all shear and axial stress - i.e., no bar elements are used (see Appendix B). The webs of the spars and ribs are treated as shear panels separated by posts which enable transfer of external loads to the structure. Inboard of the root, the type of construction dictates the need for introducing bar elements to represent the carry-through beams. Sufficient attention to the details of the carry-through structure is required to properly account for the boundary effects on the outer portion of the wing.

The configuration employs covers of stringer-reinforced titanium sheet. The internal construction uses standard titanium spars and ribs. By using the spar and rib inter section as the nodal points for the finite element model, the exposed wing is broken into ten spanwise segments and an average of five segments in the chordwise direction. Since the distribution of pressure in the chordwise direction is expected to be smooth and since there are no internal cutouts in the covers, the subdivisions in the chordwise direction should be adequate to represent the true state of stress. All the elements in the cover of the wing are well shaped, that is, the triangular



UPPER COVER



SPARS & RIBS

Figure 2 Idealization of Orbiter Wing

elements are approximately 45° isosceles triangles and the quadrilateral elements are all of aspect ratio of two or less with the exception of the last element in the trailing edge root region. This element is not connected to a fixed point on the boundary and the strain energy in the element can be expected to be low. For this reason the discrepancy between the predicted and true stress distributions can be expected to be unimportant to the overall behavior of the structure.

The spars and ribs are represented by shear panels. The axial load-carrying capacity of the web material near the covers is assumed to be accounted for in the adjacent cover elements, a factor which must be considered in the final interpretation of the results obtained in the computer program.

In constructing the geometry data for structures where the primary stresses arise from bending moments, for example wings and tails, a preliminary estimate must be made of the radius of gyration so that the behavior of the structure will be accurately reflected in the finite element model. Consider the portion of a wing cross section shown in Figure 3.

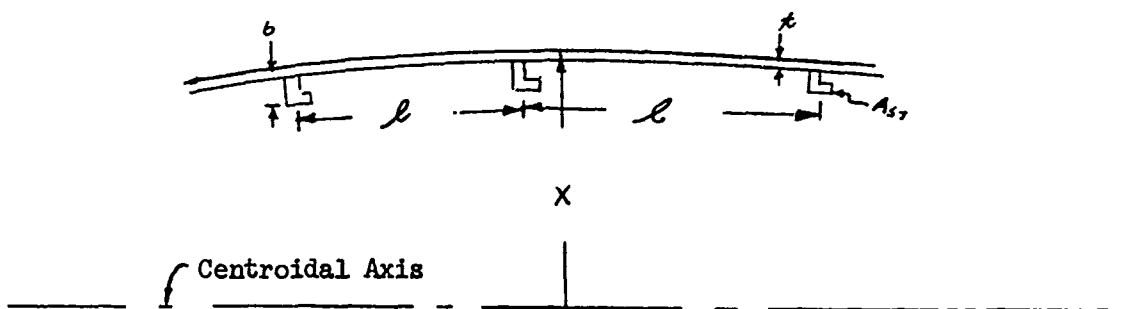


Figure 3 Portion of a Typical Wing Cross Section

Here l is the spacing between stringers, b is the depth of the stringer from the center of the cover sheet, and x is the height of the cover sheet above the centroidal axis of the wing. The moment of inertia of the finite element model about this axis should be the same as the actual wing, that is:

$$I = y^2 A = I_{xx} + \frac{1}{12} A_s t^2 + A_s x^2 + A_{st} (x - \frac{b}{2})$$

where y is the height of the element above the neutral axis of the finite element model, A is the total cross section area of the cover sheet of width l and thickness t . I_{xx} is the moment of inertia of the stringer, A_s is the sheet area between stringers and A_{st} is the area of the stringer (it is assumed that the centroid of the stringer is at $b/2$ from the center of the cover skin). Making the cross section area of the model and the actual structure the same and defining R as the ratio of stringer area to sheet area, one obtains

$$I = y^2 A = I_{xx} + \frac{1}{12} A_s t^2 + A_s x^2 + R (x - \frac{b}{2})^2 A_s$$

or neglecting b^2 compared to x^2 and thereby neglecting I_{xx} , and $\frac{1}{12} A_s t^2$ as compared to the remaining terms in the expression for inertia,

$$y^2 (1 + R) = x^2 (1 + R) - R b x$$

$$\text{or } y^2 = x^2 - \frac{Rbx}{(1+R)} .$$

Here, y is the desired height at which the finite element nodal point should be above the centerline. The thickness of the elements is now $t' = t + A_{st}/l$, the average thickness of the cover and the element idealization would be as shown in Figure 4.

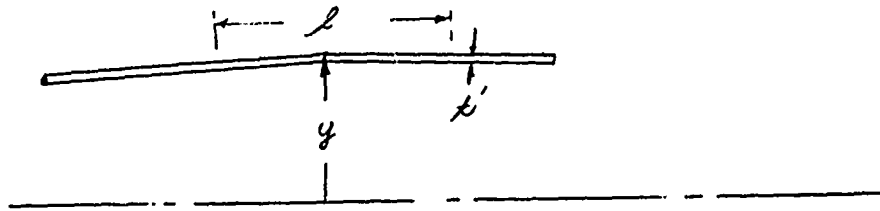
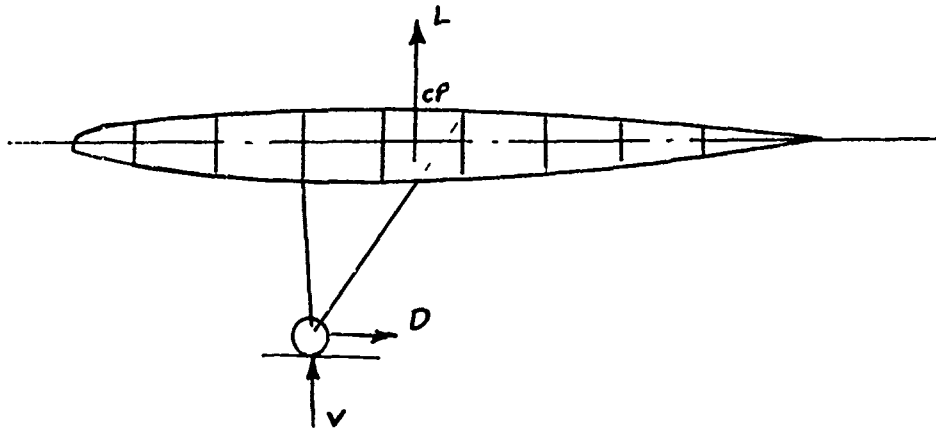


Figure 4 Finite Element Idealization of Typical Cover Element

We have now replaced the actual structure by a finite element idealization that will have the same bending stiffness. One should note that there is a slight decrease in torsional stiffness because the two covers are now closer together, and there is a slight increase in torsional stiffness because the covers contain material that is normally in the stringers. In general, if these effects are regarded as significant, the covers should be represented by a combination of bars and membrane elements.

2. Loading Conditions

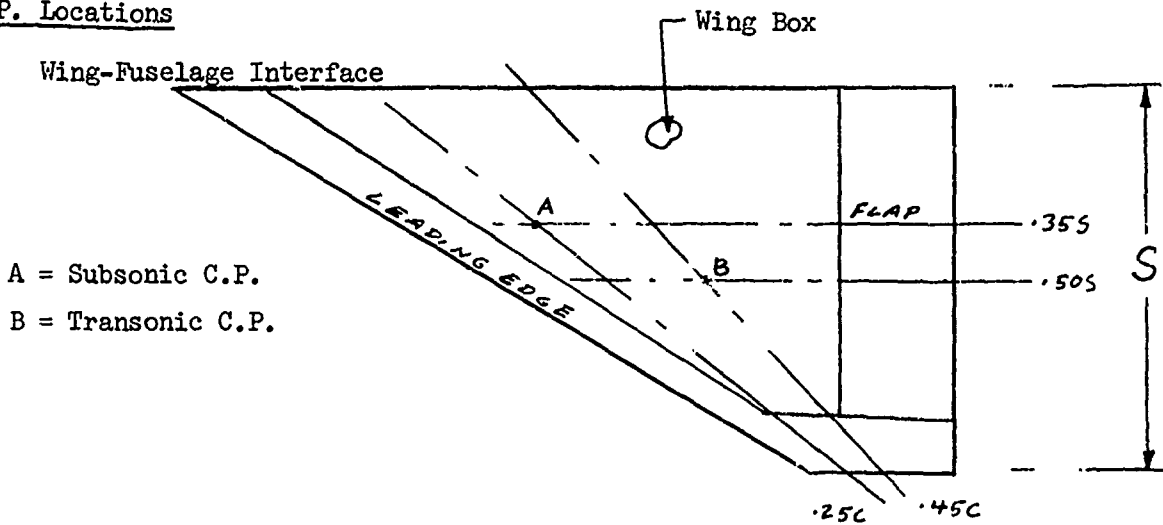
Because of the preliminary design nature of these studies, exact pressure distributions on the wing were not available. Consequently, simplified but realistic distributions had to be assumed. Five loading conditions were selected as being critical. These include: two maximum dynamic pressure conditions at positive and negative angles of attack; a 2.5g pullout condition on descent from orbit; and two landing conditions. The magnitudes of the loads are shown in Figure 5. The distribution of the loads on the exposed surface of the wing was assumed to be as shown in Figure 6. These distributions consist of a subsonic configuration and a transonic configuration. The subsonic distribution peaks rather sharply at the leading edge and tapers to zero at the trailing edge, with the



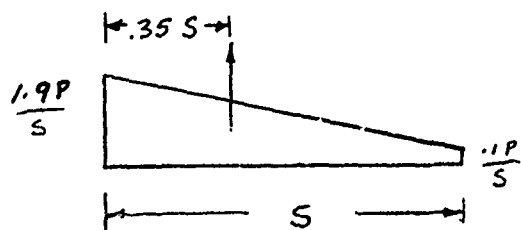
Condition	L	V	D	C P Location Fig. Ref. 6
1. Max $q \alpha (+)$	515,00	-	-	B
2. Max $q \alpha (-)$	-615,000	-	-	B
3. 2.5 g Pullout	148,000	-	-	A
4. 2-Pt Landing with Spin-Up	108,000	236,000	170,000	A
5. 2-Pt Landing with Spring - Back	108,000	265,000	-190,000	A

Figure 5 Ultimate Loads Per Side Acting on the Orbiter Wing

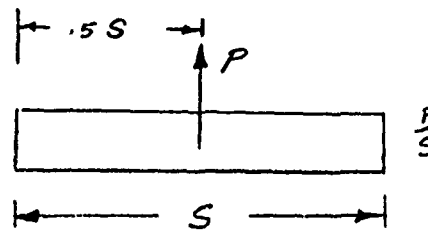
C.P. Locations



Spanwise Distribution:

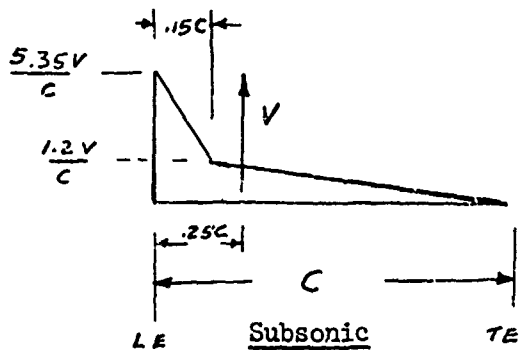


Subsonic

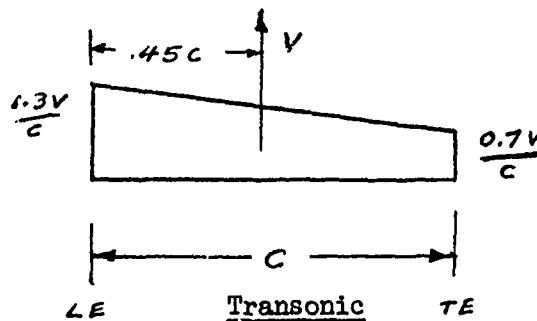


Transonic

Chordwise Distribution:



Subsonic



Transonic

Figure 6 Distribution of Applied Loads on the Orbiter Wing

spanwise distribution decreasing uniformly from root to tip. The transonic distribution, in contrast, has a linear distribution from leading to trailing edge and a constant magnitude from root to tip. These distributions are adjusted to give the correct total load and center of pressure locations for each of the loading conditions. The determination of the loads applied to a particular nodal point is based on the pressure acting at that nodal point and its associated cover area.

3. Design Criteria

The material assumed for the optimization is titanium Ti-6Al-6V-2Sn annealed having the room temperature properties given below:

$$F_{tu} = 155 \text{ ksi}$$

$$F_{ty} = 145 \text{ ksi}$$

$$F_{cy} = 148 \text{ ksi}$$

$$F_{su} = 100 \text{ ksi}$$

$$E = 17.0 \times 10^3 \text{ ksi}$$

In using the ASOP program, curves of allowable stress versus the appropriate structural index must first be developed, tabulated, and then applied to account for the instability of the cover panels (see Reference 2). The allowable stress curve used for this particular example is the curve for Y-stiffened panels shown in Figure 7. A length of thirty inches is assumed between supports.

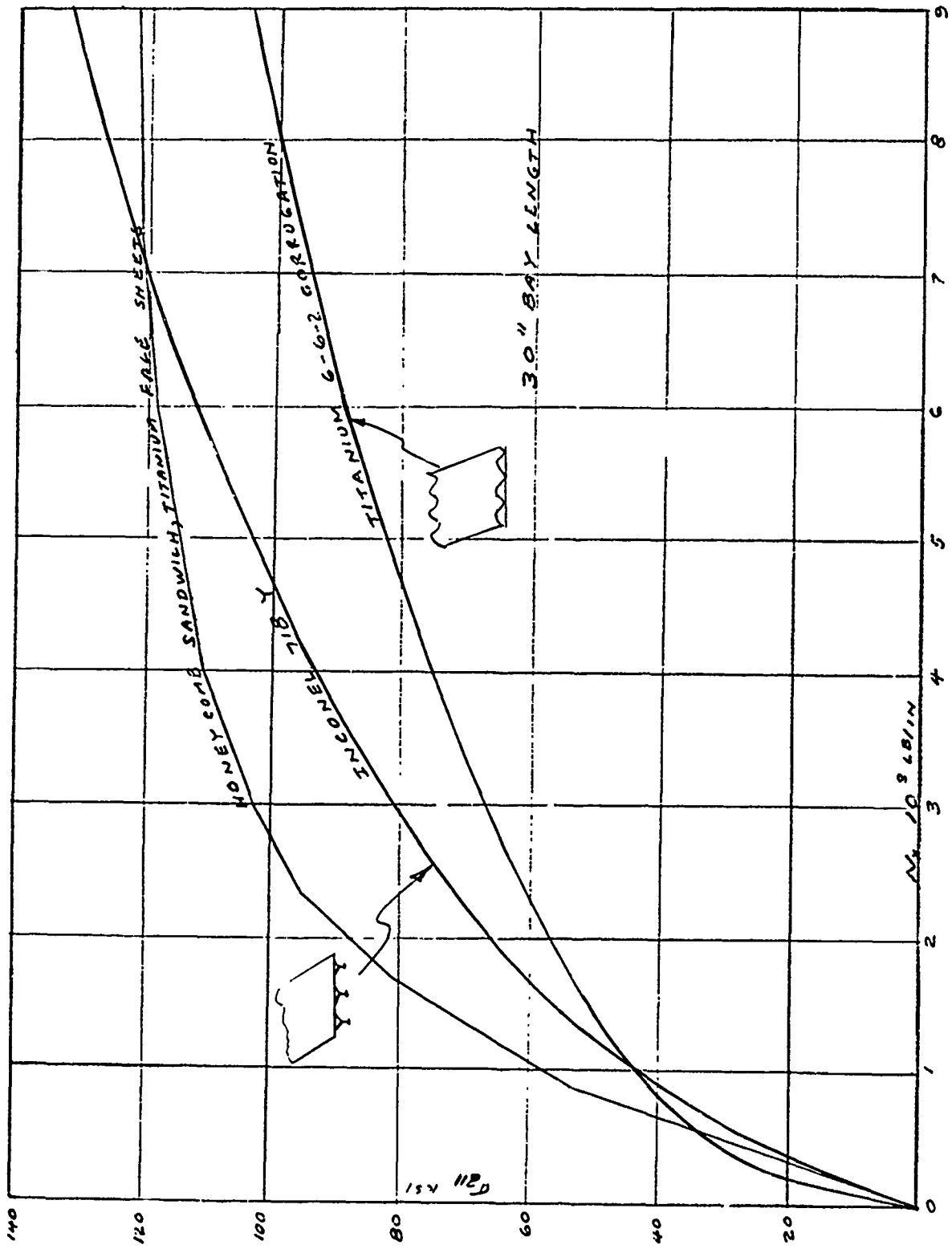


Figure 7 Conventional Cover Allowable Compressive Stress

4. Optimization Results

The wing idealization was optimized using the fully stressed design option of the ASOP program. Three iterations were performed. After three iterations the element sizes change only in the third significant figure, Therefore, for this idealization no more iterations are necessary. The top cover thicknesses are shown in Figure 8. The thicknesses increase, as expected from tip to root. The only exceptions are at a few locations near the tip where the local applied loads are high and the wing is still fairly thin, resulting in high bending stresses. The thicknesses of the spars and ribs are almost all at the minimum of .02 inches and for this reason are not shown.

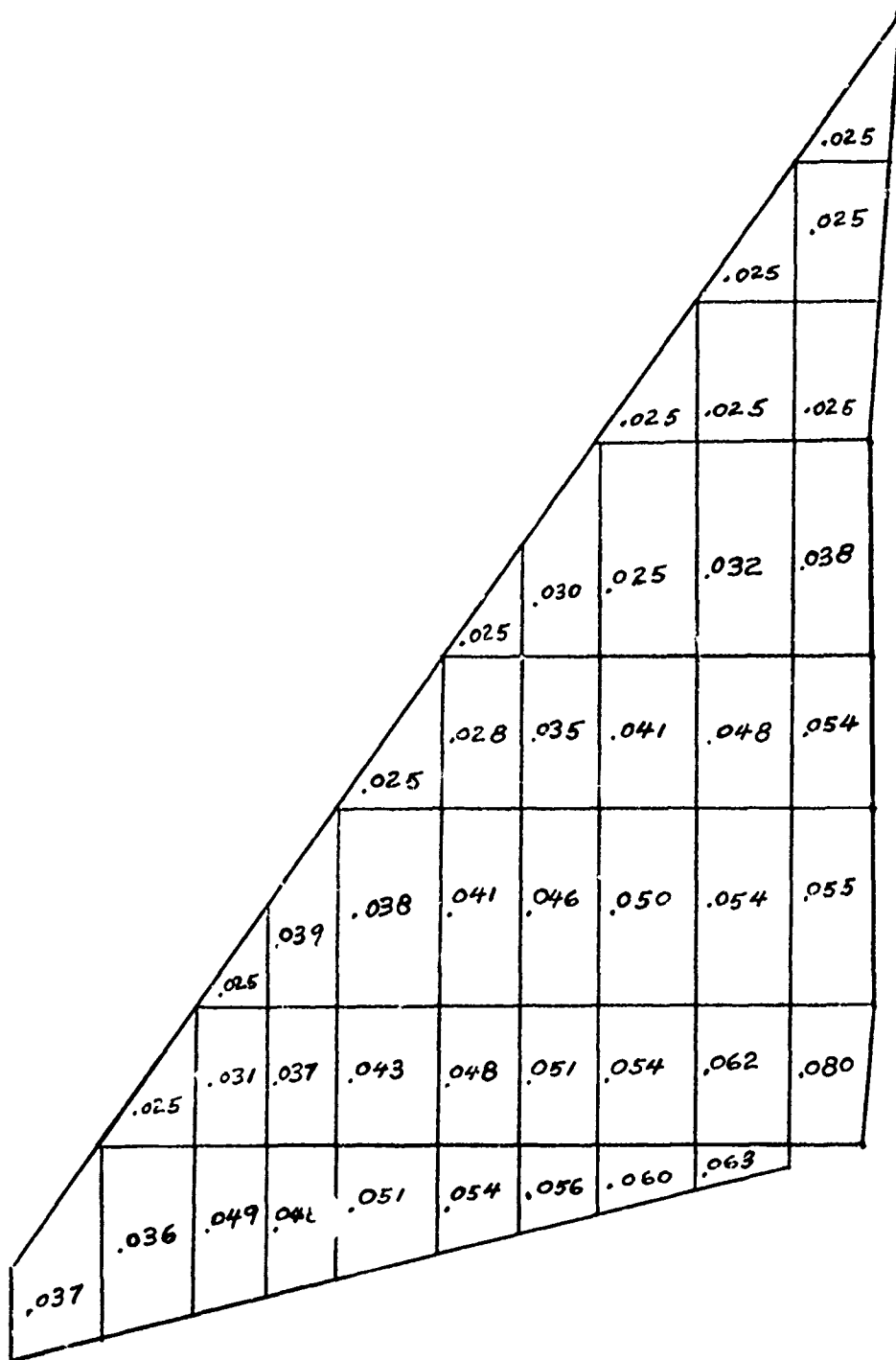


Figure 8 Thicknesses of Optimized Orbiter Wing Top Cover Elements

B. Fuselage Design Study

1. Structural Idealization

The idealization of the orbiter begins at fuselage reference station 408, (See Figure 1). Forward of this point the structure is essentially an aerodynamic fairing and is not considered as primary structure. The bulkhead station 408 is treated as a simple combination of bars, beams, and shear panels as shown in Figure 9 . The shear panels and beams allow the shear, axial load and moment from the forward tip of the fuselage to be introduced into the structure as concentrated loads at this station. The bulkhead and frame idealizations at each of the important fuselage stations is shown in Figures 10 and 11. It should be understood that the idealization includes lumped properties of the adjacent members in the real structure and not only the properties of the particular bulkhead or frame alone. Some specific comments on these structural components are now given.

The next bulkhead in the idealization is at station 548. The corresponding structure is shown in the structural arrangement drawing in Figure 11. The important point to note when comparing the idealization and the actual structural arrangement (Figure 11) at this station is the

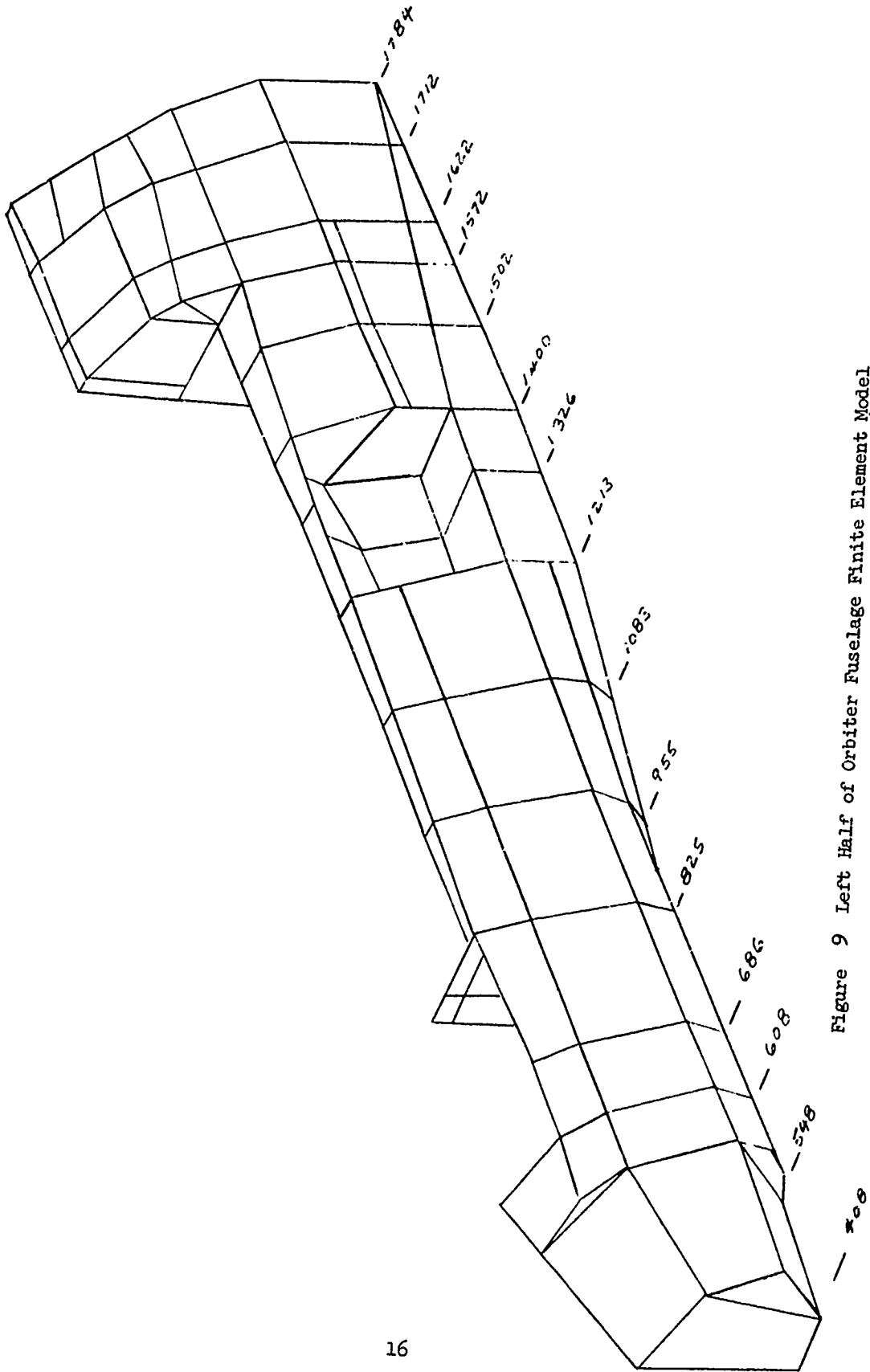


Figure 9 Left Half of Orbiter Fuselage Finite Element Model

level of detail preserved in the idealization. The number of shear panels used in the bulkhead is the minimum necessary to preserve the size and location of the cutout for the forward oxygen tank support, and to provide the backup structure for the external hydrogen tank support. There are two beam elements to maintain the approximate external contour across the top of the bulkhead.

Another point of interest is station 608. This is the point of attachment of the cabin to the fuselage. The bar element representing this attachment can be seen in the idealization. The frame is composed only of beams around the outside and bar elements on the interior. The bar elements are needed to support node 52 and to represent the lumped areas of the shear panels between the adjacent bulkheads.

The next bulkhead at station 686 serves mainly as a point of application for a portion of the distributed loads on the fuselage and also serves to break up the shear panels along the side of the fuselage into elements of reasonable aspect ratio.

Station 825 is at the bulkhead between the cabin and the cargo bay. Because the cargo bay covers are non-structural, the bulkhead is idealized only up to the hinge line of the cover. The aft cabin support is at node 83. This dictates the form of the subdivision of the bulkhead into shear panels. Again the outside of the bulkhead is defined by beam elements.

The bulkheads at stations 955 and 1083 are similar. Each is a series of beam elements around the fuselage contour and bar elements defining the central keel of the fuselage and the floor of the cargo bay. In this region the fuselage is essentially a two cell box beam. The structural idealization at

these two stations can be compared to the typical construction in this region shown in the structural arrangement drawing at station 1138 (Figure 11).

The next section of interest is at station 1213. This bulkhead supports the aft end of the main oxygen tank and receives the most forward wing spar. This is also the beginning of the air breathing engine bay. The bar from node 159 to 173 is added to stabilize one of the fuselage longerons that ends at this bulkhead and it is not structural. At this station the bulkhead has again been divided into as few shear panels as is necessary to preserve the basic behavior of the bulkhead.

The next idealized bulkhead is at 1326 where the air breathing engines are connected to the structure. The bulkhead at station 1400 is the aft booster attachment bulkhead. At this point the booster thrust loads are transferred to the orbiter making the longeron just forward of the interstage attachment point one of the heaviest members in the structure.

The bulkhead at station 1502 provides aft support for the external hydrogen tank attachment. The beam elements that make up the perimeter of the frame portion do not represent actual members in the structure, but are the result of lumping together the properties of the frames on both sides of station 1502.

The thrust structure for the main orbiter propulsion engines is provided by bulkheads at 1572 and 1622. The structural arrangement drawing (Figure 11) is presented only at 1572 which is also the end of the cargo bay and the forward attachment point for the vertical fin.

There are several interesting details in the structural idealization of this bulkhead that should be noted. One of the shear panels in the original idealization had to be replaced by a bar element because the adjacent sides of

the element were almost parallel. The main thrust structure is represented by a horizontal beam between 1572 and 1622. The forward side of this beam is represented by the bars and shear panels between nodes 273 and 257, and 274 and 259. The shear webs for the beam are represented by shear panels between the two bulkheads. Because this bulkhead represents the end of the cargo bay, support must be provided for the shear panels comprising the inner shell of the bay. These supporting nodes and the shape of the inside of the cargo bay can be seen by tracing out the nodes 274, 283, 281 and 279.

The bulkhead idealization at 1622 shows the rear end of the thrust structure beam. Also attached at this bulkhead is the support for the on orbit IO_2 tank which occupies most of the space above the center of the bulkhead.

The last two bulkheads are almost rings because of the large cutouts for the rocket exhaust. The tops of these two are attachment points for the fin.

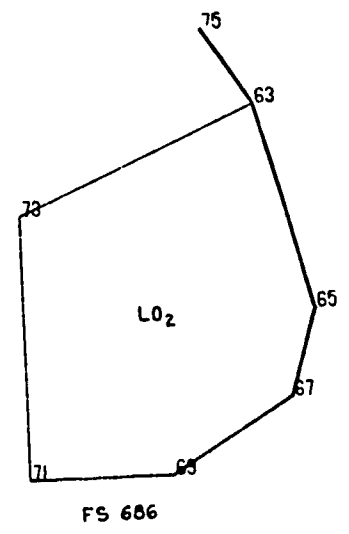
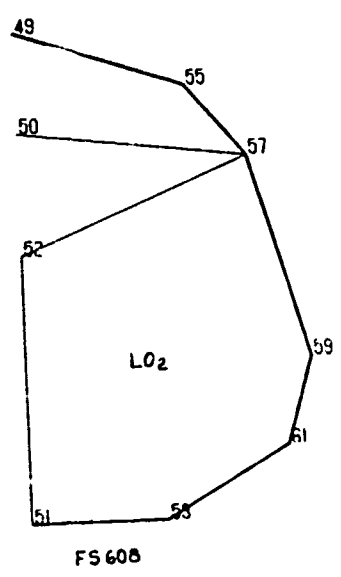
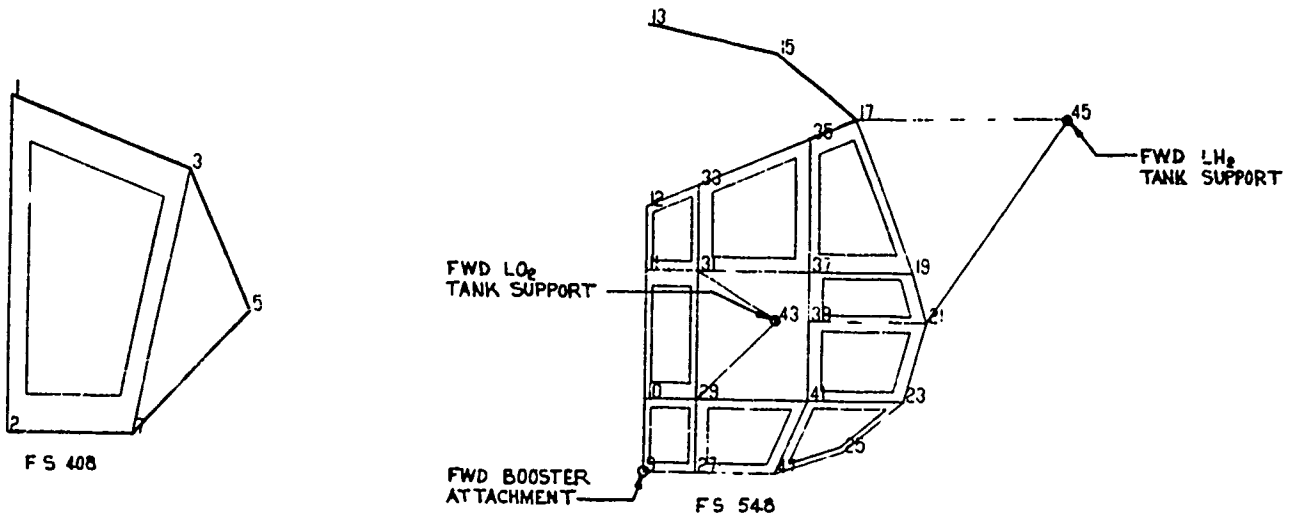


Figure 10 Fuselage Bulkhead Idealizations

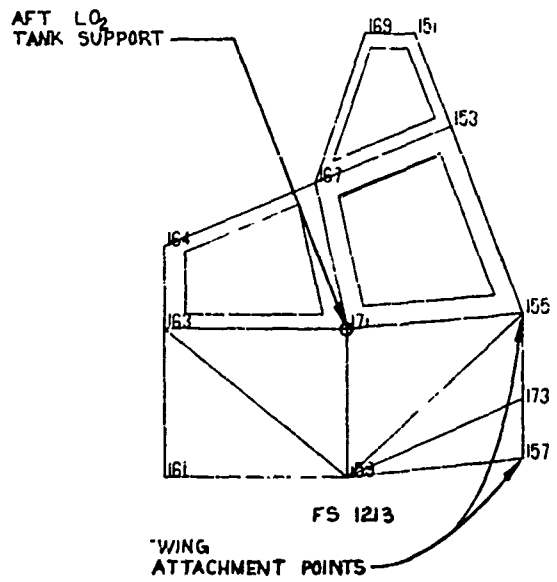
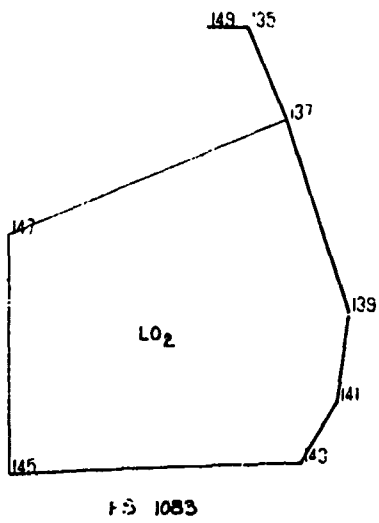
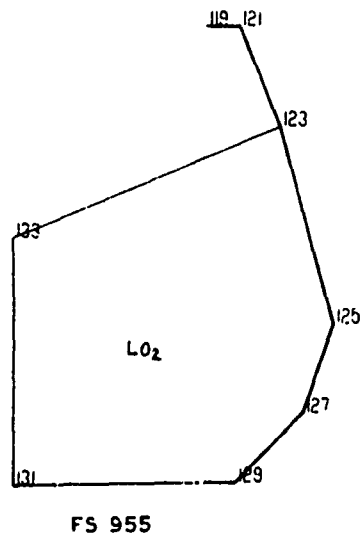
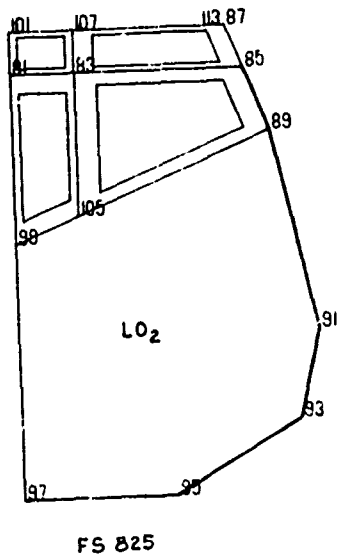


Figure 10 continued. Fuselage Bulkhead Idealizations

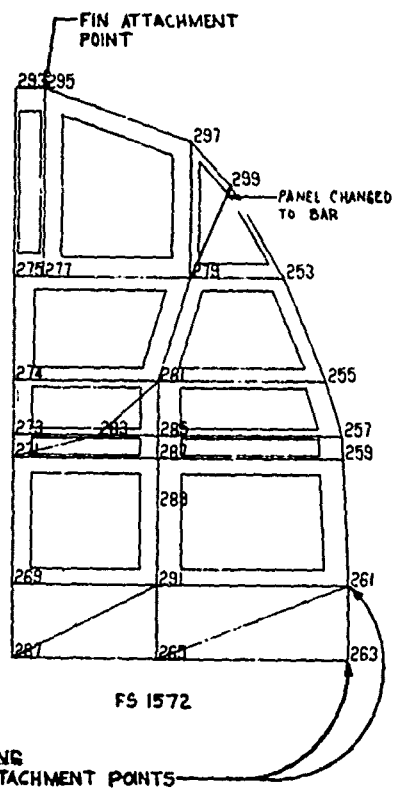
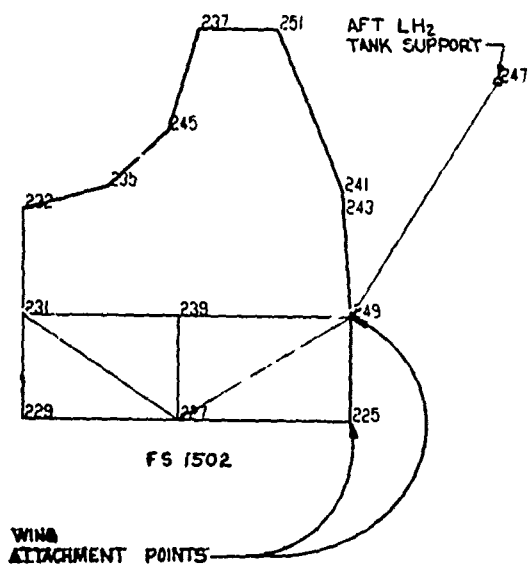
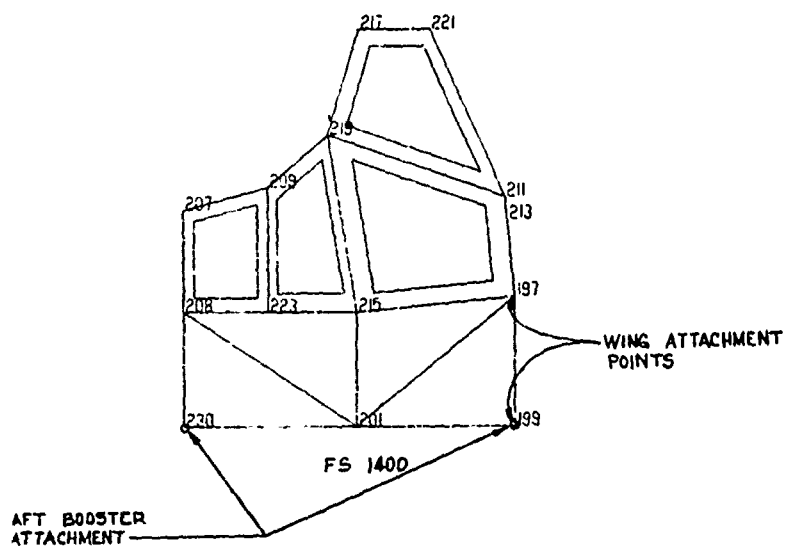
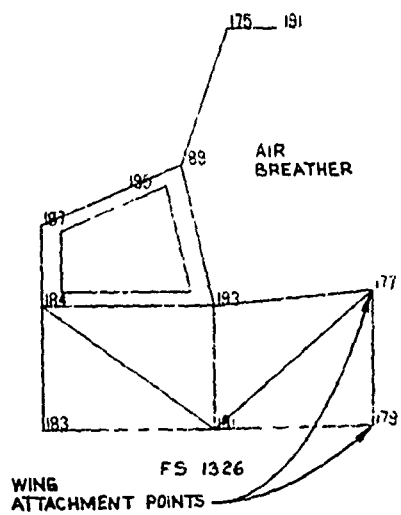


Figure 10 continued. Fuselage Bulkhead Idealizations

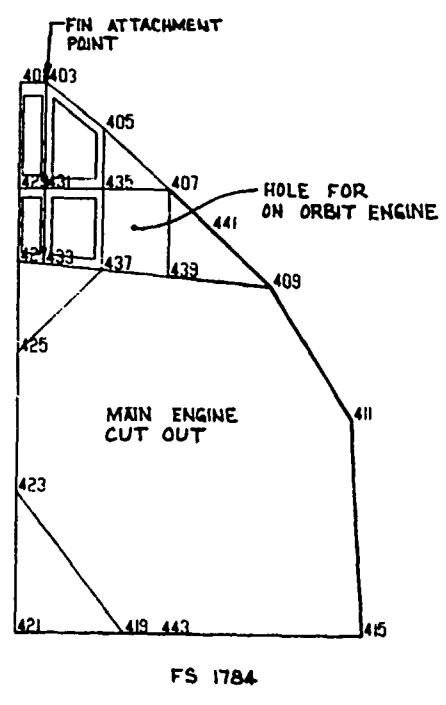
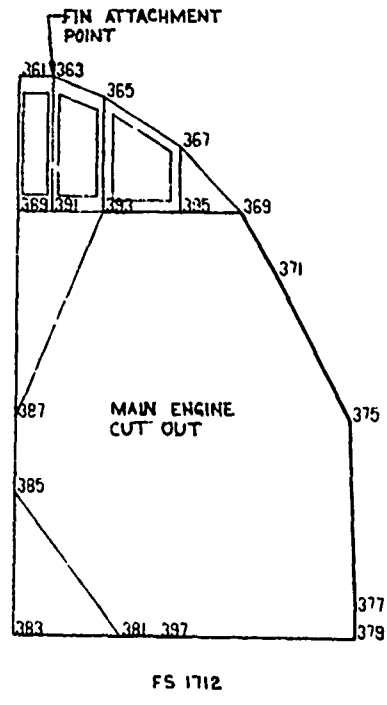
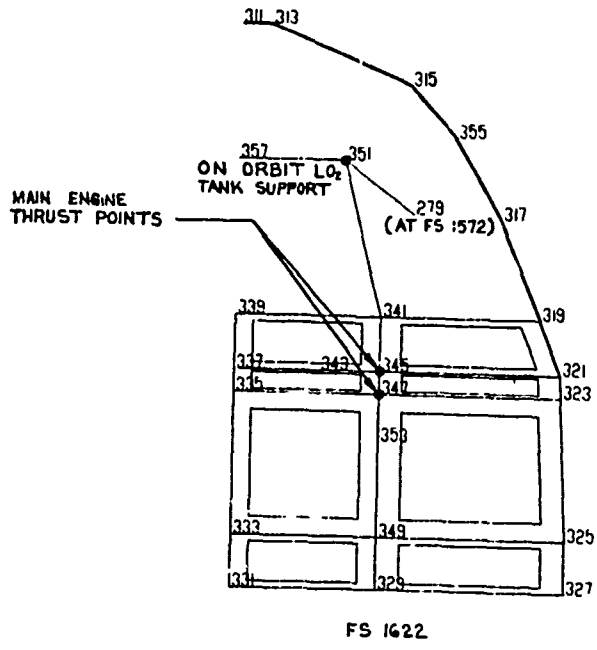


Figure 10 continued. Fuselage Bulkhead Idealizations

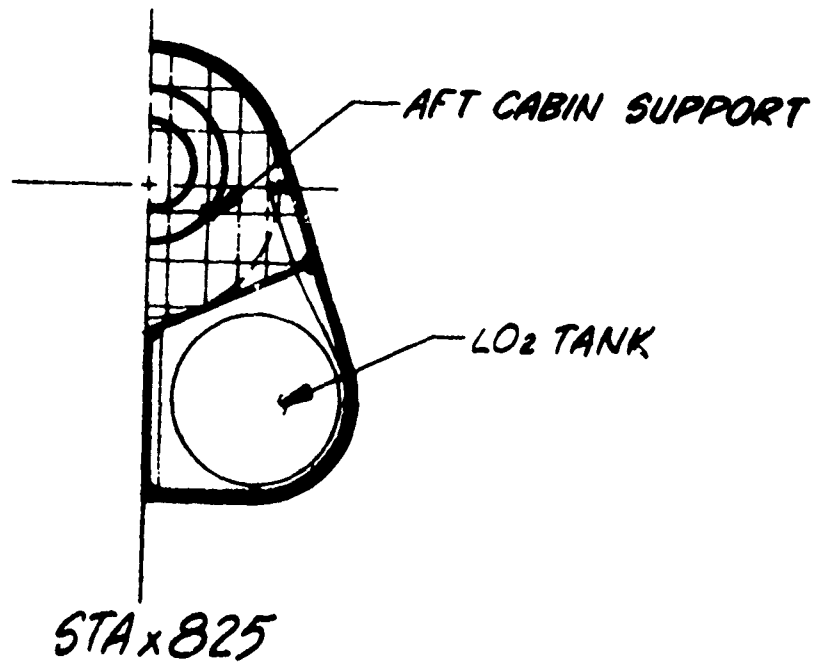
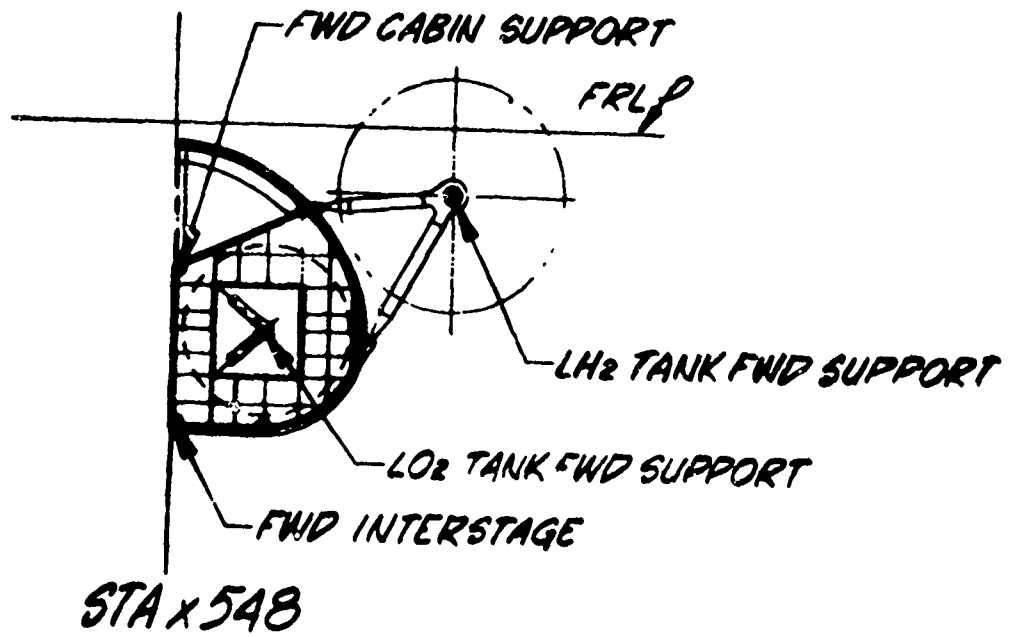
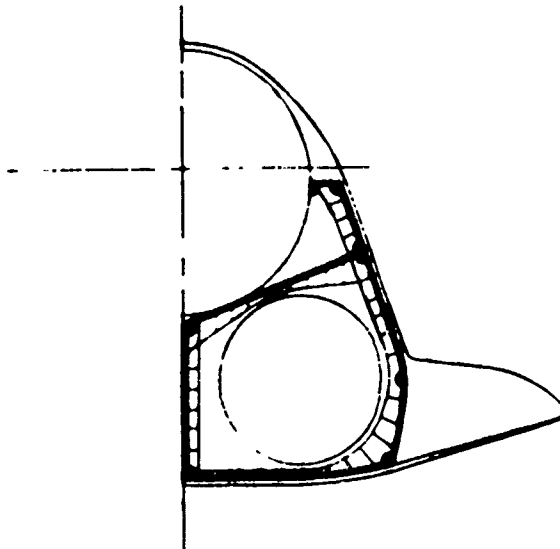
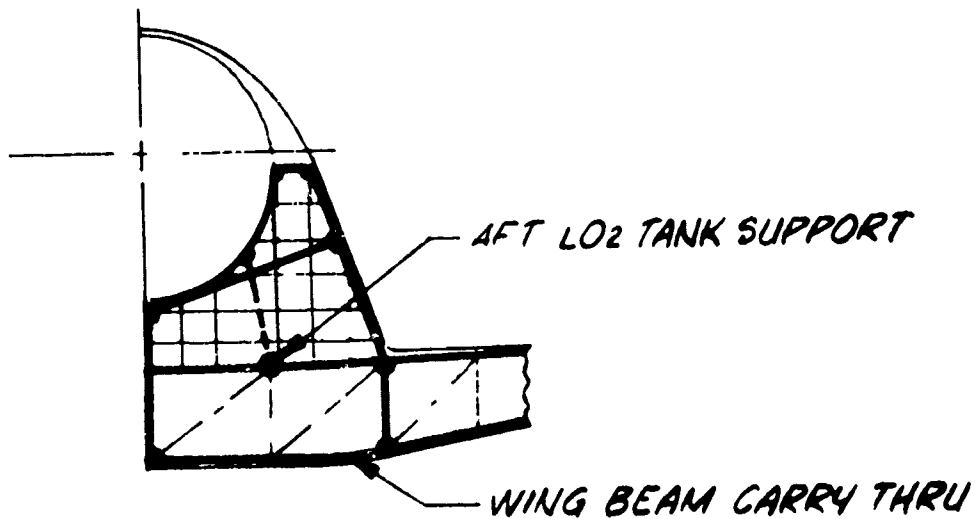


Figure 11 Fuselage Bulkhead Structural Arrangements



STA x 1138
(TYP SECTION)



STA x 1213

Figure 11 continued Fuselage Bulkhead Structural Arrangements

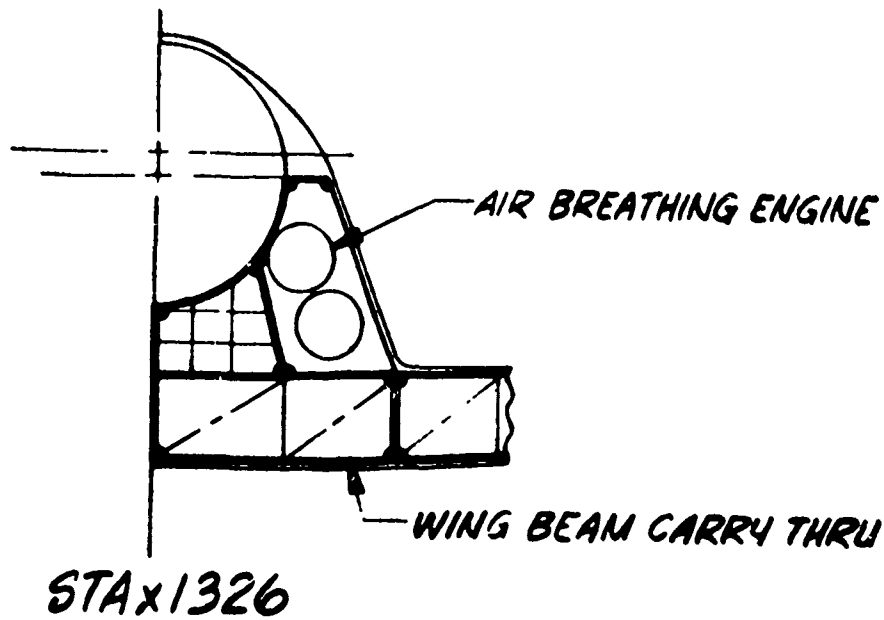
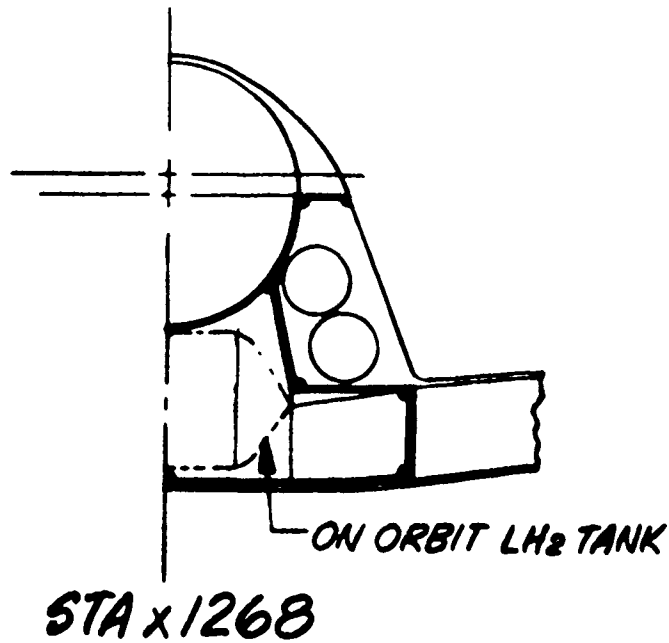


Figure 11 continued Fuselage Bulkhead Structural Arrangements

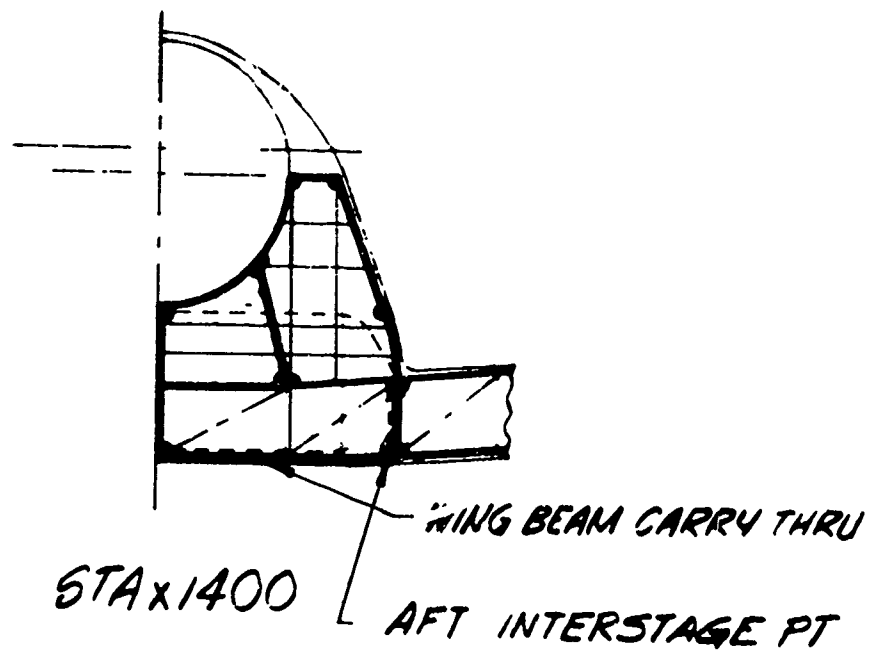
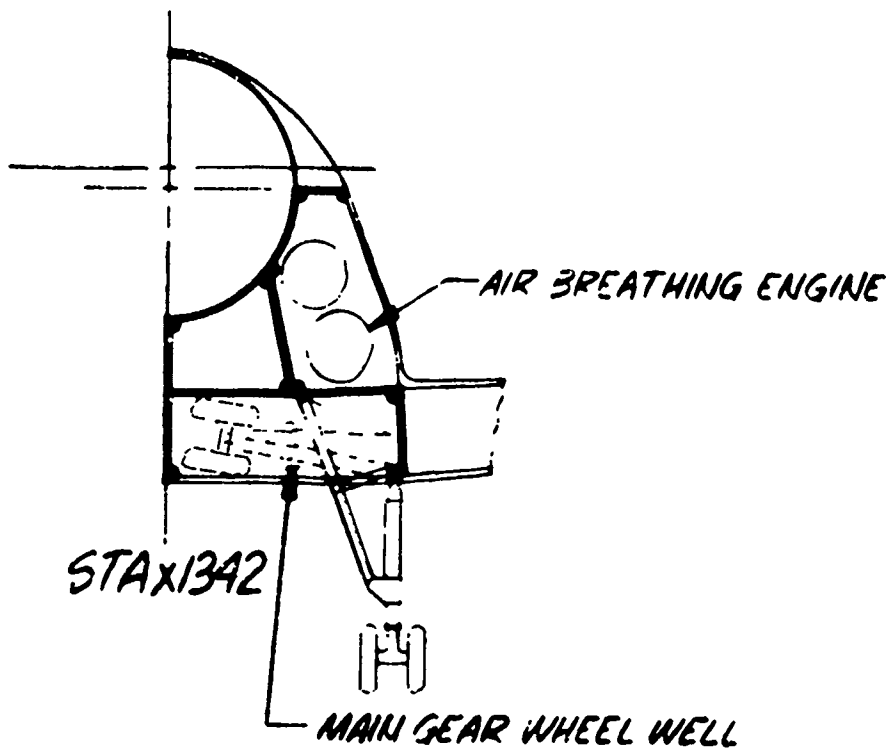


Figure 11 continued Fuselage Bulkhead Structural Arrangements

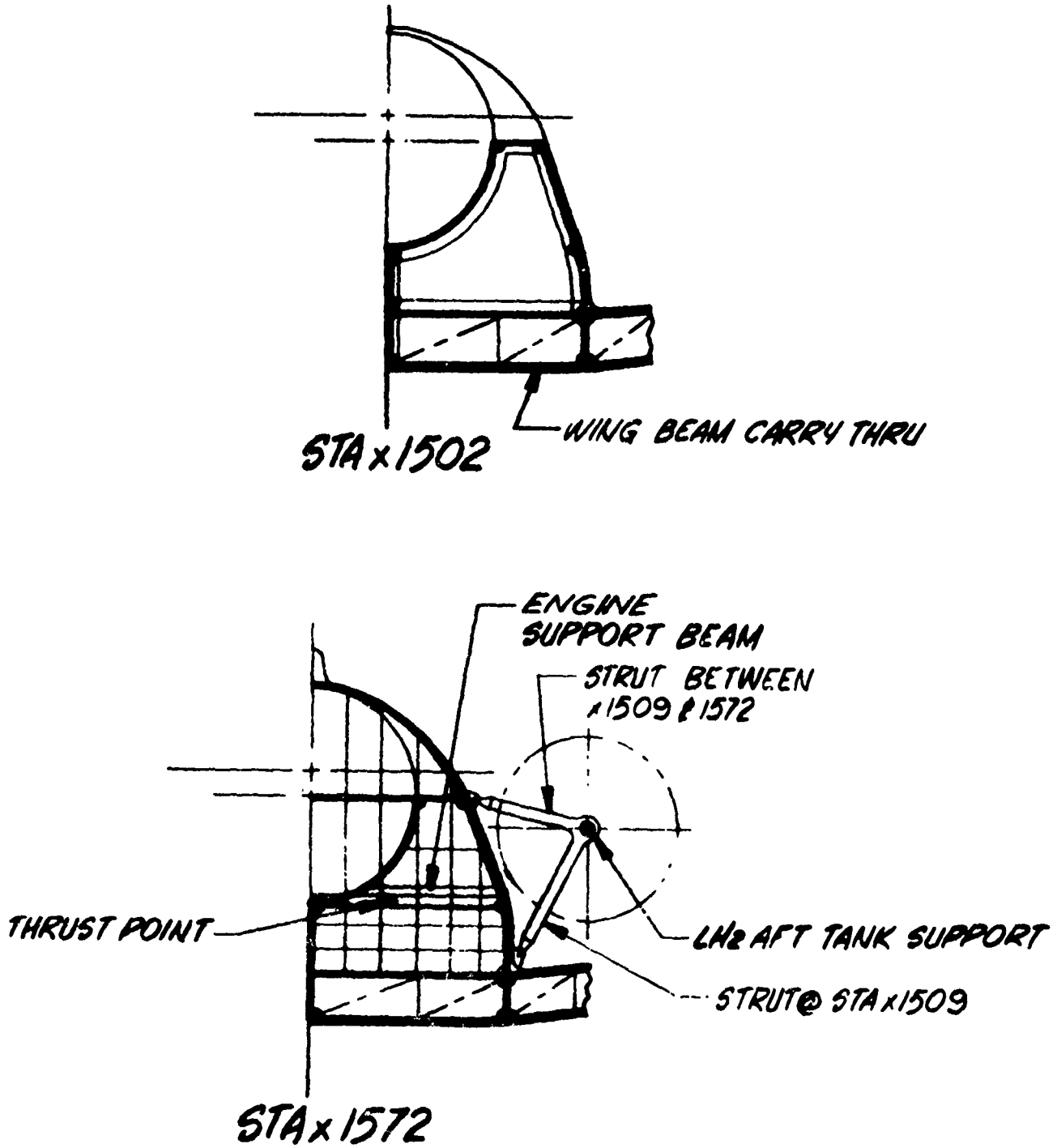
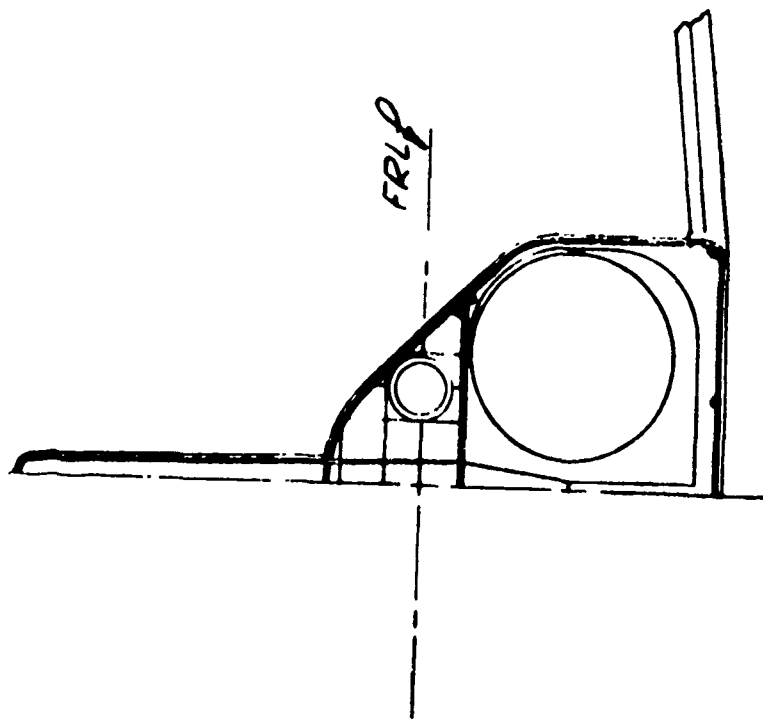
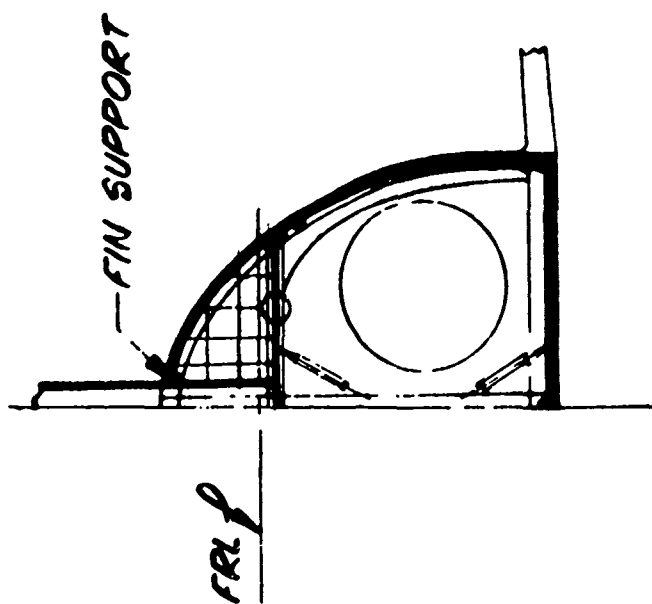


Figure 11 continued Fuselage Bulkhead Structural Arrangements



STA x 1784



STA x 1712

Figure 11 continued Fuselage Bulkhead Structural Arrangements

2. Loading Conditions

Sixteen loading conditions were selected as possibly being critical for different portions of the orbiter fuselage. A schematic of the mission profile is shown in Figure 12. The points where the different loading conditions occur are indicated. A summary of these loading conditions, with the magnitude of the safety factor for each condition, is given in Figure 13. The magnitude of the loads in each of the conditions and other relevant information is given in Figure 14. To make this information more meaningful, the envelopes of ultimate bending moment, shear, and axial loads are plotted in Figures 15, 16, and 17. In these figures the critical loading condition for each point along the fuselage is also indicated. As can be seen, the critical bending moment conditions over much of the fuselage is load condition 5 during boosted flight when the booster thrust line is several feet below the orbiter centerline.

The interface loads between the wing and fuselage and between the vertical fin and fuselage were obtained by calculating the reaction loads of the wing and tail when optimized independently as cantilevered structures. For a more rigorous analysis of these interactions it would be necessary to do a coupling analysis of the wing, tail and fuselage or alternatively analyze the entire vehicle as one structure. The interaction loads for the orbiter and booster were obtained from a previous analysis of the two vehicles together.

Numbers designate loading condition (see Figures 13, 14)

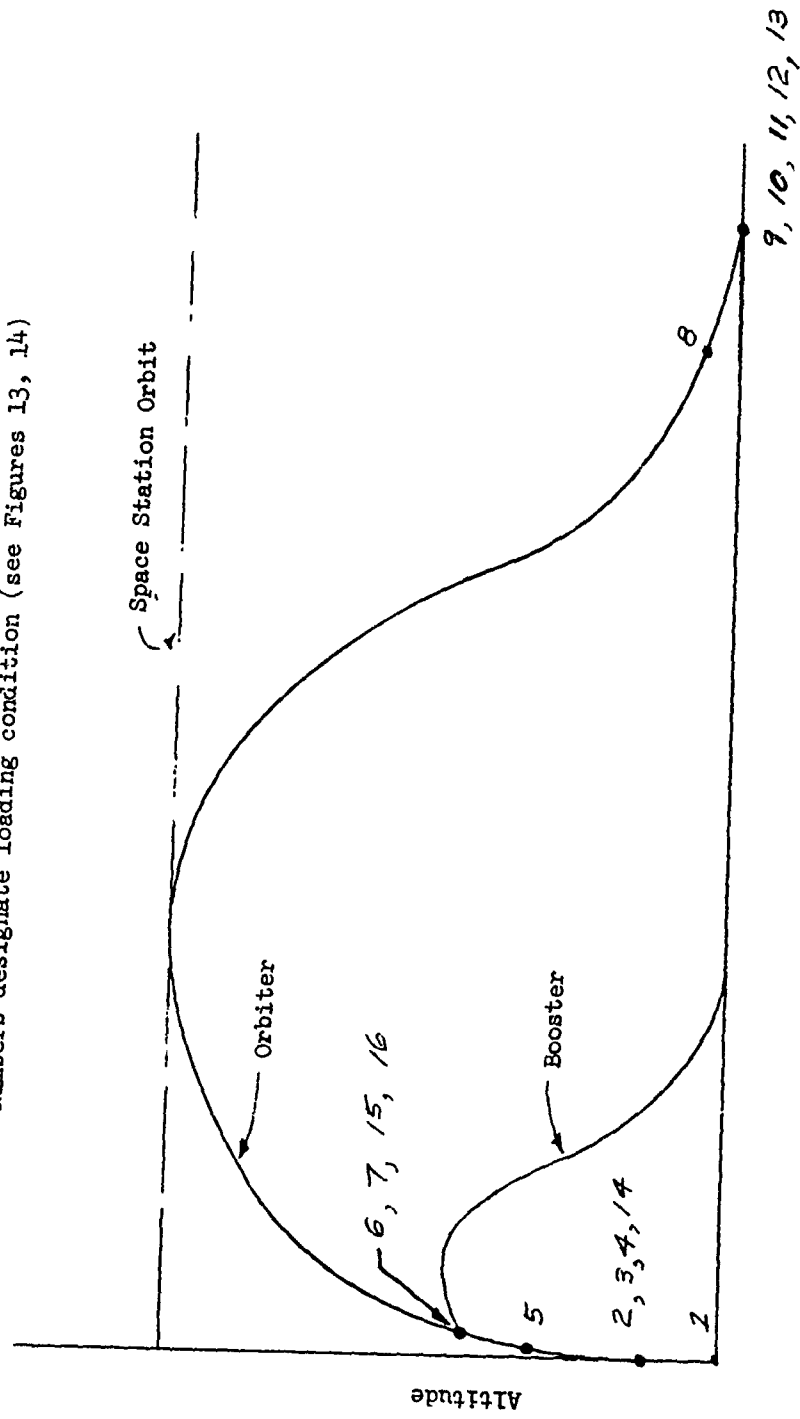


Figure 12 Mission Profile

CONDITION	SAFETY FACTOR	DESCRIPTION
1	1.4	Launch Loads with (-) Ground Winds
2	1.4	Max Q_x , Head Wind
3	1.4	Max Q_x , Tail Wind
4	1.4	Max Q_B (+ θ)
5	1.4	Initial 3G
6	1.4	End of Booster Boost
7	1.4	Orbiter Ignition
8	1.5	2.5G Pullout
9	1.5	2 Point, Tail Down, Spin-Up Landing
10	1.5	2 Point, Tail Down, Spring-Back Landing
11	1.5	2 Point, Level, Spin-Up Landing
12	1.5	Nose Gear Impact, Spin-Up Landing
13	1.5	Nose Gear Impact, Spring-Back Landing
14	1.4	Max Q_B (- θ)
15	1.4	Left Engine Only Emerg. Power Level Thrust
16	1.4	Right Engine Only Emerg. Power Level Thrust

Figure 13 H-3T Orbiter Applied Loading Conditions

ITEM	LAUNCH LOADS WITH GROUND WINDS		MAXIMUM Q (LOAD RELIEF) HEAD WIND		MAXIMUM Q (LOAD RELIEF) TAIL WIND		MAXIMUM Q (LOAD RELIEF) (+g)		INITIAL 3g		END BOOST		ORBITER IGNITION		2.5 G PULLOUT		2 POINT TAIL DOWN SPIN UP		2 POINT TAIL DOWN SPRING BACK-LANDING	
	1	2	3	4	5	6	7	8	9	10	11	12	13	14	15	16	17	18	19	20
\dot{N}_x	-1.74450	-1.32712	-1.39393	-1.42822	-2.97165	-2.97417	-1.45319	0.032185	0.532447	-1.239133										
\dot{N}_y	0.0	0.0	0.0	0.34276	0.0	0.0	0.0	0.0	0.0	0.0	0.0	0.0	0.0	0.0	0.0	0.0	0.0	0.0	0.0	0.0
\dot{N}_z	0.13866	0.63548	-0.47501	0.09631	0.36581	0.33194	-0.06812	2.50	3.095527	2.925533										
\dot{Q}_x	0.0	0.0	0.0	-0.00359	0.0	0.0	0.0	0.0	0.0	0.0	0.0	0.0	0.0	0.0	0.0	0.0	0.0	0.0	0.0	0.0
\dot{Q}_y	0.0	0.0	0.00553	0.00233	0.0	0.0	0.0	0.0	0.0	0.0	0.0	0.0	0.0	0.0	0.0	0.0	0.0	0.0	0.0	0.0
\dot{Q}_z	0.0	0.0	0.0	0.01335	0.0	0.0	0.0	0.0	0.0	0.0	0.0	0.0	0.0	0.0	0.0	0.0	0.0	0.0	0.0	0.0
MACH NUMBER	1.1	1.1	0.95	1.04	5.5	5.4	5.4	0.3	5.4	5.4	5.4	5.4	5.4	5.4	5.4	5.4	5.4	5.4	5.4	5.4
ALTITUDE	26,000	26,000	26,000	26,000	161,568	206,992	207,000	5000	5000	5000	5000	5000	5000	5000	5000	5000	5000	5000	5000	5000
WEIGHT	962,015	962,015	962,015	962,015	962,015	962,015	962,015	962,015	962,015	962,015	962,015	962,015	962,015	962,015	962,015	962,015	962,015	962,015	962,015	962,015
Xco	1016	1016	1016	1016	1016	1016	1016	1016	1016	1016	1016	1016	1016	1016	1016	1016	1016	1016	1016	1016
Yco	380	380	380	380	380	380	380	380	380	380	380	380	380	380	380	380	380	380	380	380
Zco	63.4	63.4	63.4	63.4	157.1	185.4	185.4	185.4	185.4	185.4	185.4	185.4	185.4	185.4	185.4	185.4	185.4	185.4	185.4	185.4
TIME	0	585.9	43.5	523.3	0.0	0.0	0.0	0.0	0.0	0.0	0.0	0.0	0.0	0.0	0.0	0.0	0.0	0.0	0.0	0.0
DYNAMIC PRESSURE	5,900,000	6,302,600	6,302,600	6,302,600	6,112,428	5,064,000	5,064,000	5,064,000	5,064,000	5,064,000	5,064,000	5,064,000	5,064,000	5,064,000	5,064,000	5,064,000	5,064,000	5,064,000	5,064,000	5,064,000
THRUST (BOOSTER)																				
ITEM	11	12	13	14	15	16	17	18	19	20										
\dot{N}_x	1.000236	0.21442	-0.039341	-1.42822	-0.720597	-0.720597	-0.720597	-0.720597	-0.720597	-0.720597										
\dot{N}_y	0	0	0	-0.34276	-0.09214	-0.09214	-0.09214	-0.09214	-0.09214	-0.09214										
\dot{N}_z	2.957700	1.904974	2.05601	0.09651	-0.008393	-0.008393	-0.008393	-0.008393	-0.008393	-0.008393										
\dot{Q}_x	-0.982493	-0.010147	0.38722	0.08359	0	0	0	0	0	0										
\dot{Q}_y				-0.01335	0	0	0	0	0	0										
MACH NUMBER				1.04	5.4	5.4	5.4	5.4	5.4	5.4										
ALTITUDE	5.1	5.1	5.1	28,000	207,000	207,000	207,000	207,000	207,000	207,000										
WEIGHT	237,851	237,851	237,851	962,015	962,015	962,015	962,015	962,015	962,015	962,015										
Xco	1262	1262	1262	1016	1016	1016	1016	1016	1016	1016										
Yco	402	402	402	380	380	380	380	380	380	380										
Zco				63.4	185.4	185.4	185.4	185.4	185.4	185.4										
TIME																				
DYNAMIC PRESSURE				6,302,600	6,302,600	6,302,600	6,302,600	6,302,600	6,302,600	6,302,600										
THRUST (BOOSTER)																				

Figure 14 Summary of Applied Loading Conditions

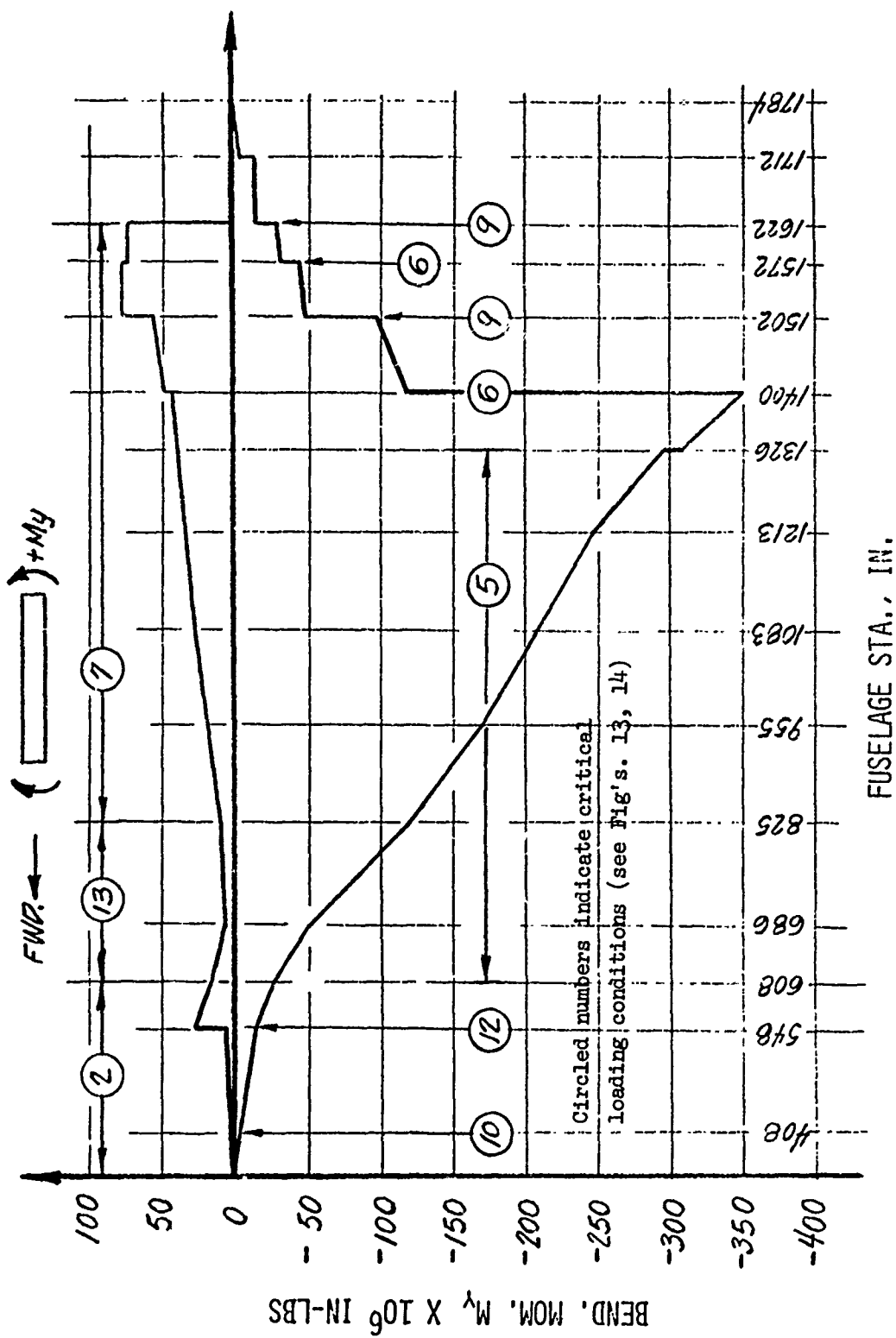


Figure 15 H-3T Orbiter Fuselage Ultimate Bending Moment Envelope

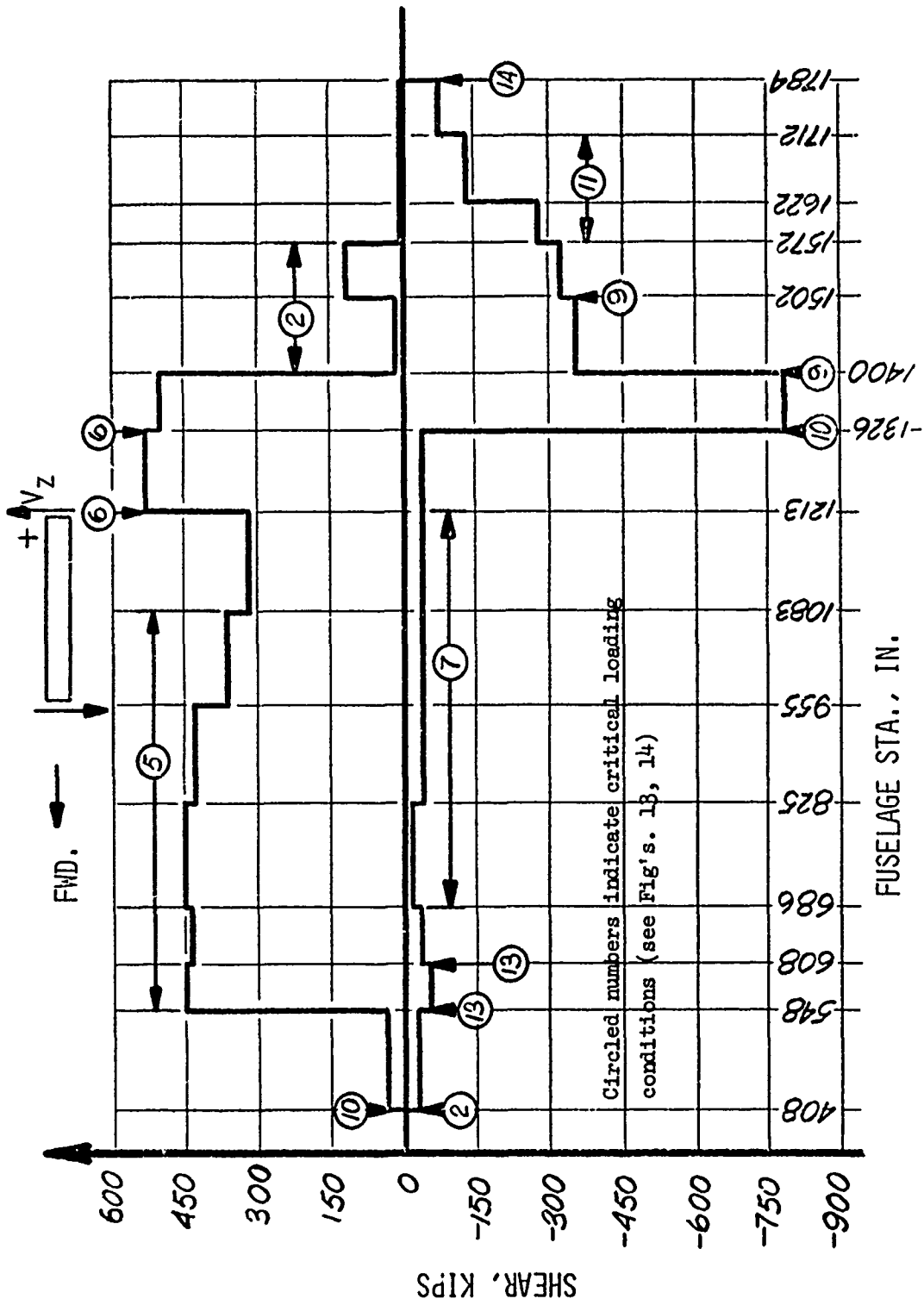


Figure 16 H-3T Orbiter Fuselage Ultimate Vertical Shear Envelope

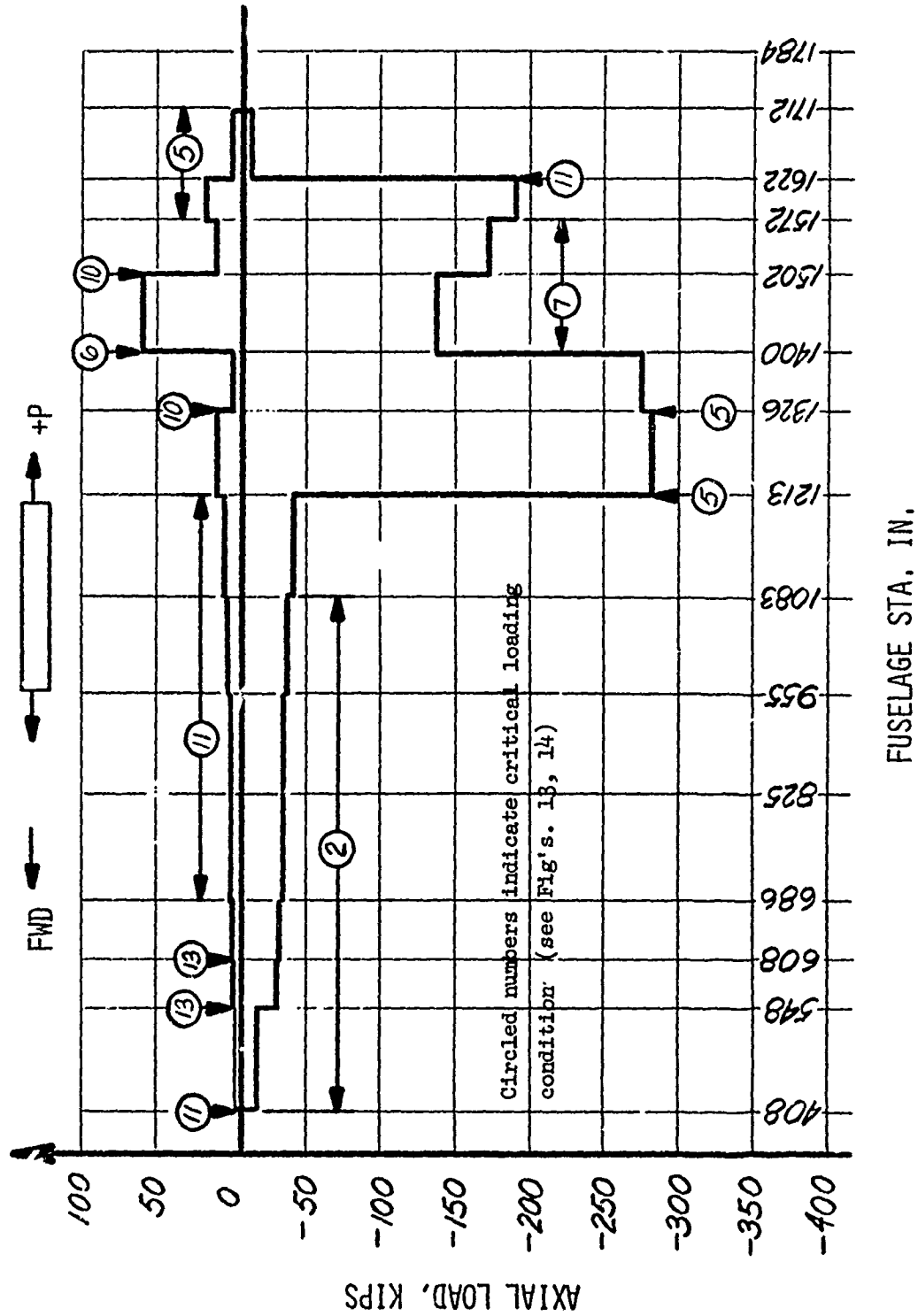


Figure 17 H-3T Orbiter Fuselage Ultimate Axial Load Envelope

3. Design Criteria

The orbiter fuselage is assumed to be made of the same material as the wing as given previously. But because in the fuselage large portions of the skin are in diagonal tension the elastic properties of most of the shear panels must be modified. The only exceptions are several panels near the main propulsion engines which are heavily loaded and therefore thick enough to resist shear buckling.

To modify the shear stiffness of the panels in diagonal tension, the shear modulus was reduced to 75% of its normal value. The justification for this is based on the graph in Figure 18 which is copied from Reference 3.

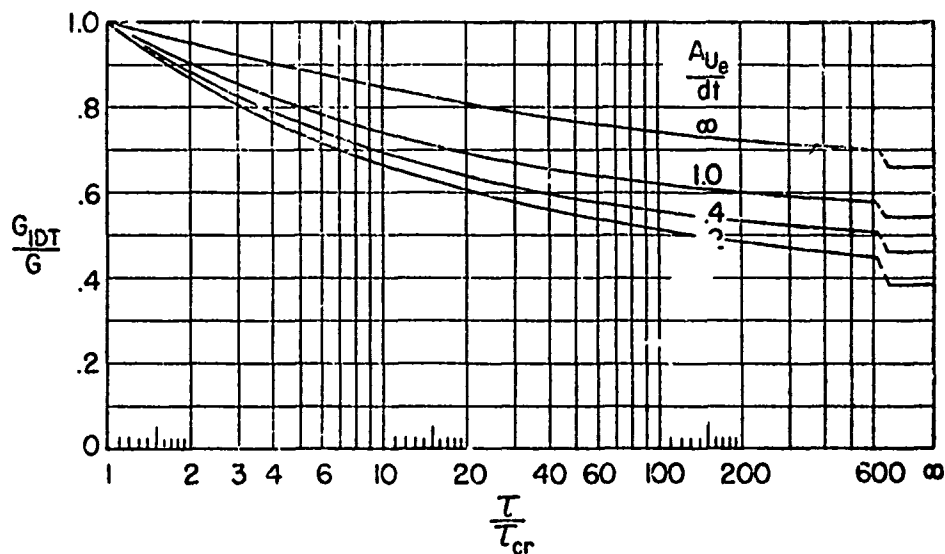


Figure 18 Modulus Ratio for Buckled Elastic Web

In this figure τ/τ_{cr} is the ratio of shear stress to shear buckling stress. G_{IDT}/G is the ratio of effective shear modulus for the buckled panel to shear modulus for an unbuckled panel. A_{Ue}/dt is the effective area of the upright (in this particular case a ring) to the cross section area of the sheet. For a wide range of τ/τ_{cr} , the shear stiffness ratio is about .75 when the upright area is large compared to the sheet area between uprights. In the ASOP program the input is in terms of E (Young's modulus) and ν Poisson's ratio and it is therefore not possible to specify G directly. Instead orthotropic material properties are specified for all shear panels in diagonal tension.

The failure criteria used for the fuselage are the standard criteria in ASOP, that is, maximum shear stress in the shear panels and maximum allowable axial stress in the bar elements that are buckle-resistant. The buckling stress criteria used for optimization for those bar elements that are not well supported, for example the hydrogen tank attachment struts, is shown in Figure 19.

4. Optimization Results

Two separate optimizations of the fuselage were performed starting with different initial element sizes. The initial optimization started with a size distribution that was generated by hand. First, the structure was sized using simple strength of materials formulas and the ultimate applied moment and shear envelopes. Using these rough sizes a finite element analysis was performed to obtain accurate internal loads. With these internal loads the structure was again resized by hand. The weight of the resulting finite element model was 17,200 pounds. Except for a few minor exceptions, all the shear panels in the structure were at the minimum allowable thickness. The structure was then optimized using ASOP. Three iterations were performed using the fully stressed design option in the program. The weights of the structure for the iterations were 12,150 lbs., 12,200 lbs. and 12,080 lbs. The major

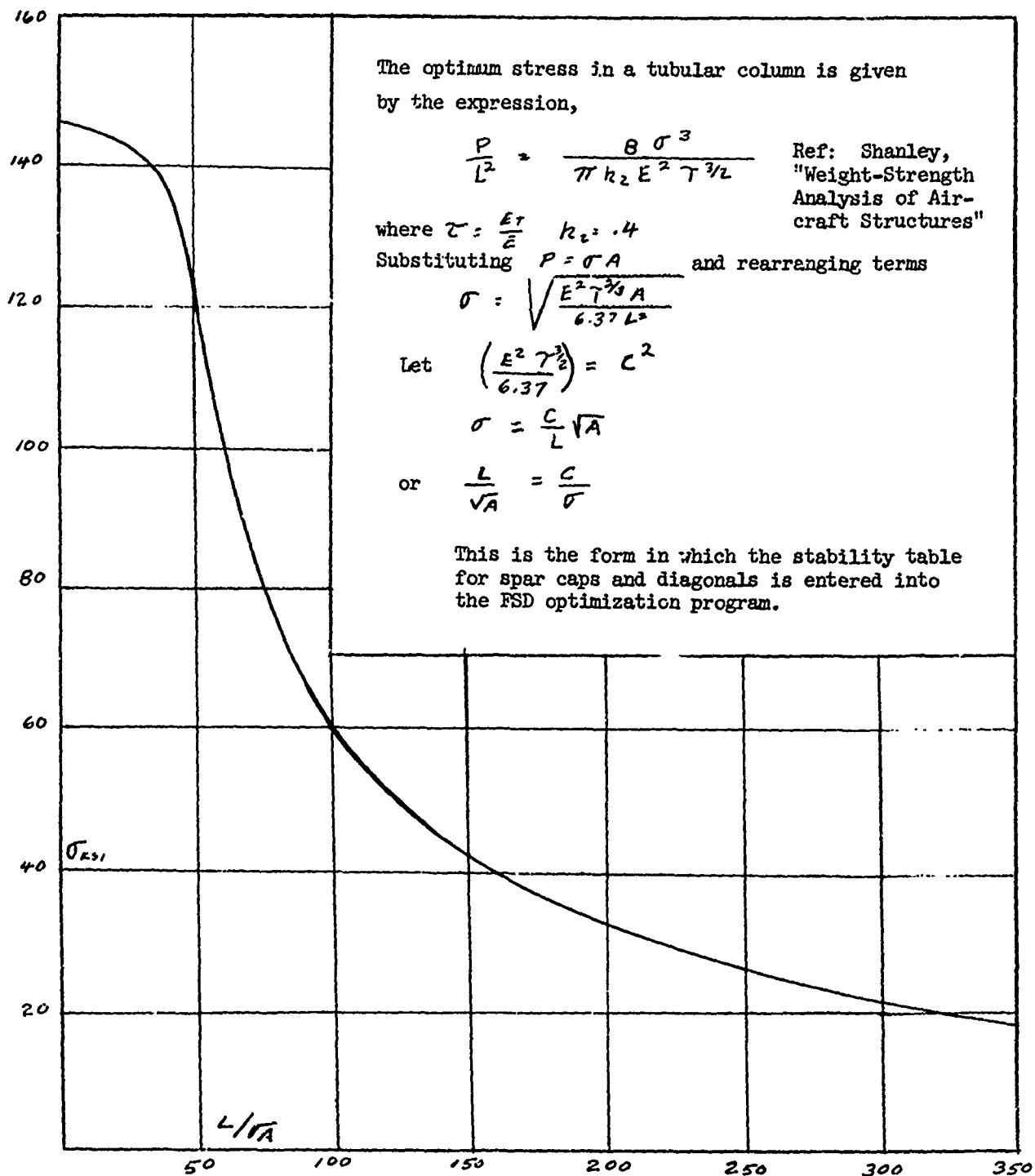


Figure 19 Allowable Compressive Stress for Bar Elements

difference between the final structure weighing 12,080 lbs. and the initial structure weighing 17,200 lbs. was the areas of the frame elements which were not initially sized for the applied loads, instead only approximate values were used. The most interesting results of the optimization are the sizes of the main longerons. For convenience these longerons have been identified in Figure 20. The areas of these longerons at the start of the optimization and after the final iterations are given in Figure 21. Also the critical loading condition is indicated. As can be expected from an examination of ultimate bending moment envelope, load condition 5 is the critical condition over most of the length for those longerons near the top and bottom of the fuselage.

In general, the longerons near the forward and aft ends of the fuselage are at minimum area. From a comparison of the starting size and the final size it can be seen that the initial calculations using strength of materials theory and a single finite element analysis gave a material distribution that is fairly close to the final distribution. This is important because it indicates that the ASOP program is generating material distributions similar to those that would be generated by more traditional methods.

After this first optimization of the structure was completed, another one was performed starting with uniform element gages. The results of this exercise are shown in Figure 22 where the longeron areas are given in a form similar to Figure 21. This time the areas for the first resizing and the last resizing are given. Seven iterations were performed in all. The critical loading conditions are the same as before and are not repeated in the figure. The weight of the structure after three iterations is essentially the same as the final weight in the previous case. The weight after seven iterations is 11,750 pounds. An examination of these final element sizes and

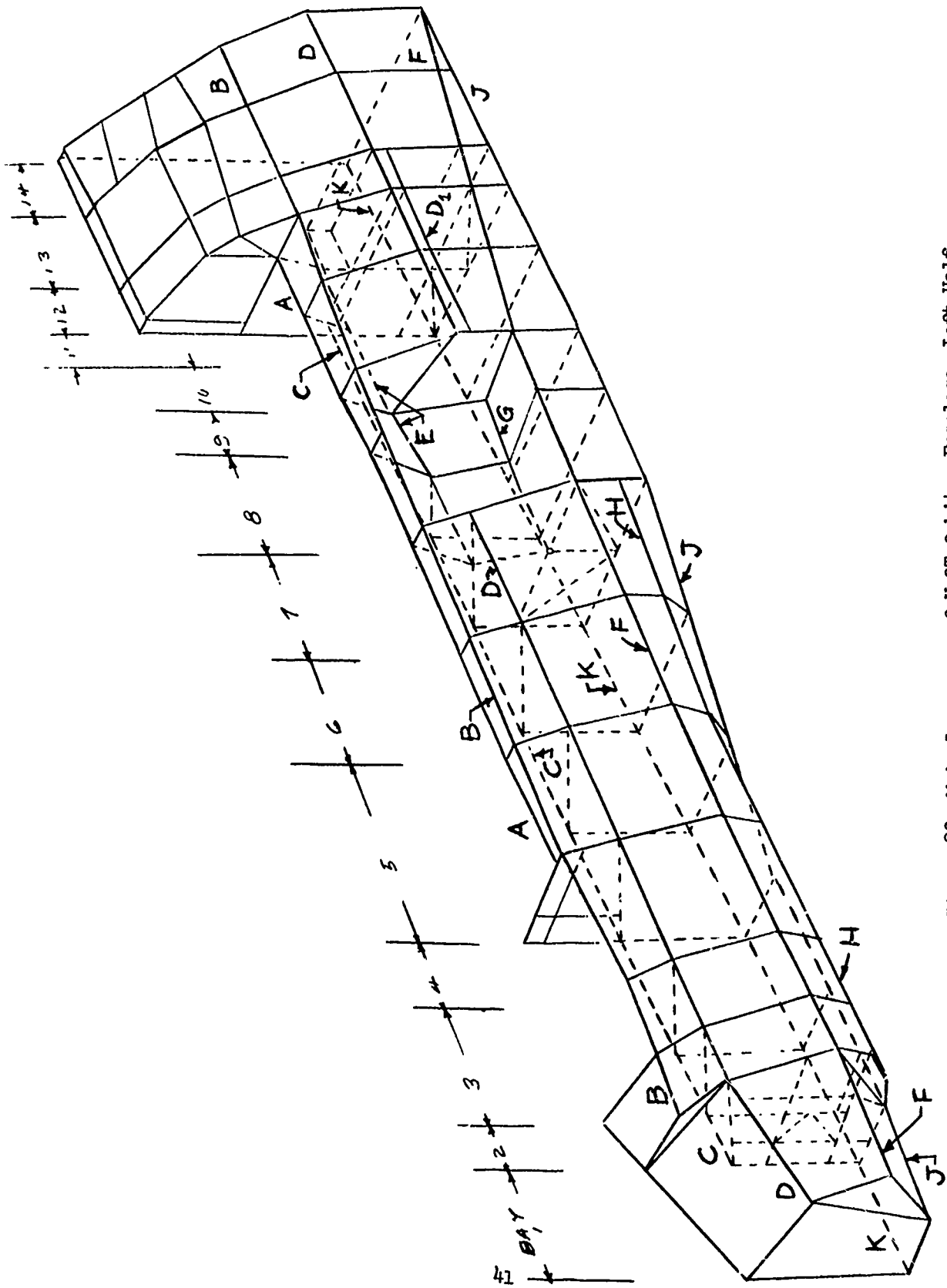


Figure 20 Main Longerons of H-3T Orbiter Fuselage, Left Half

LOCATION	LONGERON NUMBER	BAY NUMBER													
		1	2	3	4	5	6	7	8	9	10	11	12	13	14
UPPER INBOARD	A			FIRST RESIZING STH LAST	.63	1.38	1.73	2.14	1.91	1.10	.48				
	B		.42	.42	.88	1.37	1.77	1.83	1.81	1.54	.94	.51	.40	.40	.40
	C		.43	.52	.98	1.42	1.53	1.56	1.80	1.73	1.29	.79	.40	.40	.40
UPPER KEEL	D		.43	.59	1.08	1.49	1.51	1.61	1.99	1.95	1.48	.93	.40	.40	.40
	D ₁		.40	.40	.40	.40	1.21	1.39	1.49	.95	1.31	.91	.40	.40	.40
	E		.40	.40	.40	.40	.84	1.15	1.81	1.63	1.77	1.14	.51	.40	.40
LOX TANK	F		.40	.40	.57	.74	.42	1.59	2.43	2.26	2.01	1.11	.61	.40	.40
	G		.40	.40	.40	.40	.40	.62	.79	.91	1.56	.79	.40	.40	.40
	H		.40	.40	.40	.40	.40	.64	.95	1.16	1.69	.89	.40	.40	.40
LOWER OUTBOARD	I		.40	.40	.40	.40	.40	.66	1.10	1.08	1.30	.64	.40	.40	.40
	J		.40	.40	.40	.40	.40	6.40	1.78	.40	.40	.60	.40	.40	.40
	K		.40	.40	.40	.40	.40	6.41	1.81	.40	.40	.59	.40	.40	.40
LOWER KEEL	L		.40	.40	.40	.40	.40	6.42	1.82	.40	.40	.59	.40	.40	.40
	M		.40	.40	.40	.40	.40	.95	1.03	.40	.40	.60	.40	.40	.40
	N		.40	.40	.40	.40	.40	.97	1.06	.40	.40	.59	.40	.40	.40
LOWER KEEL	O		.40	.40	.40	.40	.40	.98	1.08	.40	.40	.59	.40	.40	.40
	P		.40	.40	.40	.40	.40	.61	.61	.64	.40	.40	.40	.40	.40
	Q		.40	.40	.40	.40	.40	.44	.44	.64	.40	.40	.40	.40	.40
LOWER KEEL	R		.40	.40	.40	.40	.40	.40	.40	.64	.40	.40	.40	.40	.40
	S		.40	.40	.40	.40	.40	.40	.40	.64	.40	.40	.40	.40	.40
	T		.40	.40	.40	.40	.40	.40	.40	.64	.40	.40	.40	.40	.40

Figure 22 Areas for the H-3T Longerons After Optimization Starting with Uniform Sizes

the final sizes for the previous example shows that the two designs are essentially the same even though the starting points were different.

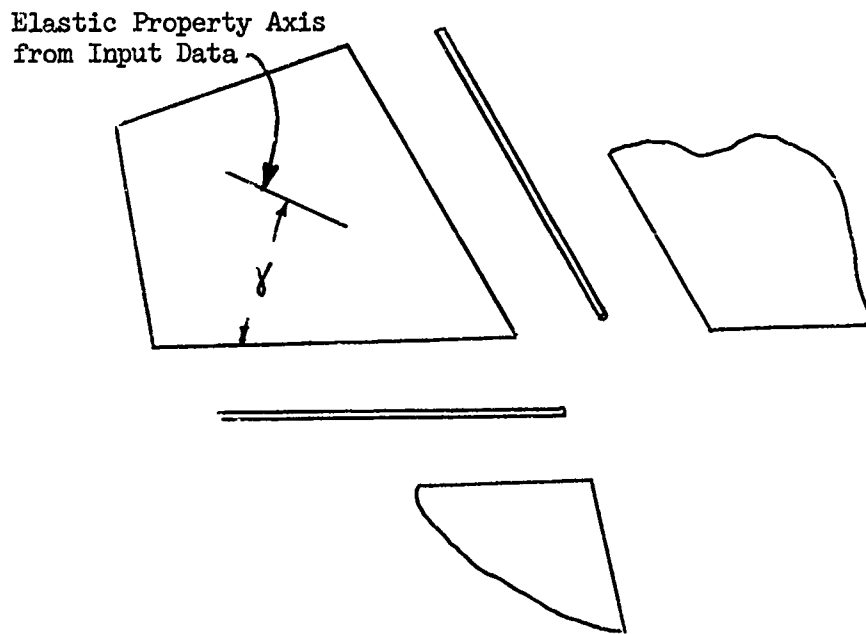
REFERENCES

1. Dwyer, W., Emerton, R., and Ojalvo, I., "An Automated Procedure for the Optimization of Practical Aerospace Structures", Volume I Theoretical Development and Users Information, AFFDL TR-70-118, April 1971.
2. Shanley, F. R., "Weight Strength Analysis of Aircraft Structures", Dover Publications, Inc., New York, N.Y. (1960).
3. Kuhn, P., and Peterson, J., "A Summary of Diagonal Tension Part 1 Methods of Analysis", NASA TN 2661, May 1952.

APPENDIX A

Modifications for Anisotropic Load Distribution

Equation 4-2 pages 48 and 49 of reference 1 has been modified to give the correct load distribution for anisotropic construction. This has been accomplished by using the values of E in the direction of the element edges in formula 4.2.6.



This is done by pre and post multiplying the elastic constant A_{ij} by the transformation matrix

$$\begin{bmatrix} \cos^2 \gamma & \sin^2 \gamma & \sin \gamma \cdot \cos \gamma \\ -\sin^2 \gamma & \cos^2 \gamma & \sin \gamma \cdot \cos \gamma \\ \sin 2\gamma & -\sin 2\gamma & \cos 2\gamma \end{bmatrix} \quad \text{where } \gamma$$

is the angle between the elastic property axis and the side of the element.

This gives a new elastic property matrix \tilde{A}_{ij} . From \tilde{A}_{ij} , E can be easily extracted.

APPENDIX B

ORTHOTROPIC BEHAVIOR OF INTEGRALLY STIFFENED PANELS

A non-isotropic structure frequently encountered in present day aircraft structural analysis is the integrally stiffened panel, Fig. 23. The following derivation is made with the purpose of applying the anisotropic finite elements herein described to problems of analysis of such structures, where the stiffeners form a regularly distributed orthotropic gridwork. This work does not consider the flexural behavior of such structures but does describe the in-plane mechanics of deformation.

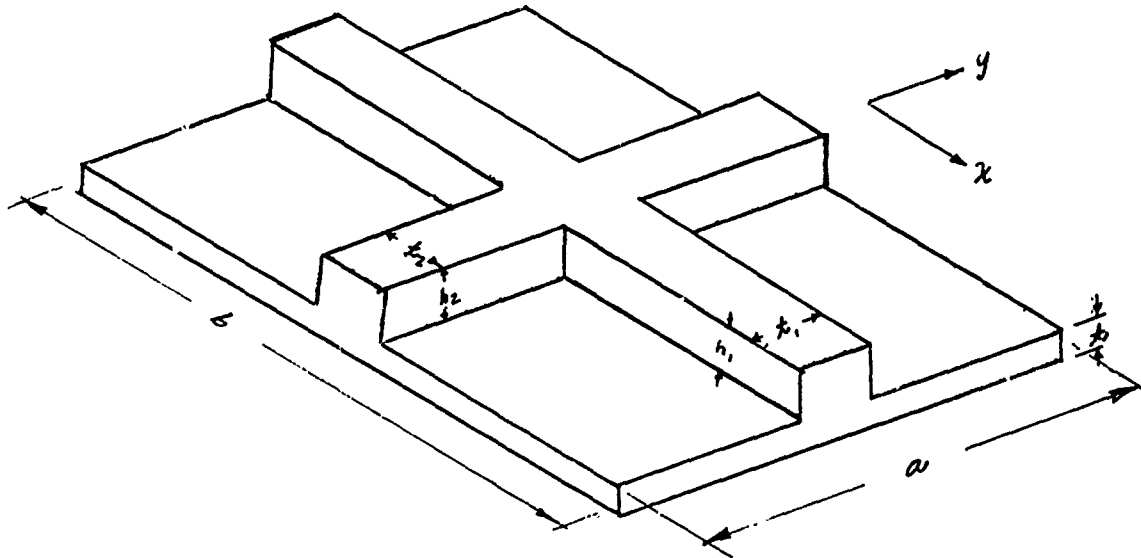


Fig. 23. Integrally Stiffened Panel

b = Stiffener spacing in x direction

a = Stiffener spacing in y direction

$A_1 = h_1 t_1$ area of stiffener in x direction

$A_2 = h_2 t_2$ area of stiffener in y direction

$$\beta_1 = \frac{A_1}{at} = \frac{\text{Stiffener area} - x \text{ direction}}{\text{Plate area} - x \text{ direction}}$$

$$\beta_2 = \frac{A_2}{bt} = \frac{\text{Stiffener area} - y \text{ direction}}{\text{Plate area} - y \text{ direction}}$$

$$\lambda_1 = 1 + \beta_1(1 - \nu^2)$$

$$\lambda_2 = 1 + \beta_2(1 - \nu^2)$$

Consider the strain energy of the module pictured on P. 47

$$U = \frac{t}{2} \int_0^a \int_0^b (\sigma_x \epsilon_x + \sigma_y \epsilon_y + \tau_{xy} \gamma_{xy}) dx dy \quad (a)$$

$$+ \frac{A_1}{2} \int_0^b \sigma_1 \epsilon_1 dx + \frac{A_2}{2} \int_0^a \sigma_2 \epsilon_2 dy$$

Where σ_x , σ_y , τ_{xy} , ϵ_x , ϵ_y , γ_{xy} are stress and strain components in the plate. σ_1 , ϵ_1 are stress and strain of the stiffener in the x direction while σ_2 , ϵ_2 are the stress and strain of the stiffener in the direction.

Assumptions:

1. Stress, and therefore strain, does not vary with coordinates (i.e. independent of x, y).
2. For compatibility of the structural components we must assume $\epsilon_1 = \epsilon_x$ and $\epsilon_2 = \epsilon_y$

Stress-Strain Relations:

$\left\{ \begin{array}{c} \sigma_x \\ \sigma_y \\ \tau_{xy} \end{array} \right\}$	$\frac{E}{1-\nu^2}$	$\frac{\nu E}{1-\nu^2}$	$\left\{ \begin{array}{c} \epsilon_x \\ \epsilon_y \\ \gamma_{xy} \end{array} \right\}$	$(b1)$
	$\frac{\nu E}{1-\nu^2}$	$\frac{E}{1-\nu^2}$	$\left\{ \begin{array}{c} \epsilon_x \\ \epsilon_y \\ \gamma_{xy} \end{array} \right\}$	
			$\left\{ \begin{array}{c} \epsilon_x \\ \epsilon_y \\ \gamma_{xy} \end{array} \right\}$	

$\left\{ \begin{array}{c} \sigma_1 \\ \sigma_2 \end{array} \right\}$	E	$\left\{ \begin{array}{c} \epsilon_1 \\ \epsilon_2 \end{array} \right\}$	$(b2)$
		E	

Substituting the stress-strain relations into the strain energy equation and performing the indicated volume integrations, we obtain the following expression for strain energy.

$$U = \frac{abt}{2} \left[\frac{E\lambda_1}{1-\nu^2} \epsilon_x^2 + \frac{E\lambda_2}{1-\nu^2} \epsilon_y^2 + \frac{2E\nu}{1-\nu^2} \epsilon_x \epsilon_y + G \gamma_{xy}^2 \right] \quad (c)$$

In order to obtain generalized stress components we must define a strain energy density function with respect to the plate volume in order that integration over the plate volume yields the total strain energy in the stiffened panel.

$$U = \int_{VOL. PL.} U_0 dV = abt U_0 \quad (d)$$

It must be noted that the modified Hooke's Law that follows is based on this step. When the modified Hooke's Law is used to derive a stiffness or flexibility matrix, the integration must be done over the plate volume only. The strain energy density is therefore:

$$U_0 = \frac{1}{2} \left[\frac{E\lambda_1}{1-\nu^2} \epsilon_x^2 + \frac{E\lambda_2}{1-\nu^2} \epsilon_y^2 + \frac{2E\nu}{1-\nu^2} \epsilon_x \epsilon_y + G \gamma_{xy}^2 \right] \quad (e)$$

The generalized stress-strain relations are obtained by differentiating the strain energy density with respect to the components of the strain tensor, for example:

$$\bar{\sigma}_x = \frac{\partial U_0}{\partial \epsilon_x} \quad (f)$$

The resulting modified stress-strain relations are:

$$\begin{Bmatrix} \bar{\sigma}_x \\ \bar{\sigma}_y \\ \bar{\tau}_{xy} \end{Bmatrix} = \begin{bmatrix} \frac{E\lambda_1}{1-\nu^2} & \frac{\nu E}{1-\nu^2} & 0 \\ \frac{\nu E}{1-\nu^2} & \frac{E\lambda_2}{1-\nu^2} & 0 \\ 0 & 0 & G \end{bmatrix} \begin{Bmatrix} \epsilon_x \\ \epsilon_y \\ \gamma_{xy} \end{Bmatrix} \quad (9)$$

$$\begin{Bmatrix} \epsilon_x \\ \epsilon_y \\ \gamma_{xy} \end{Bmatrix} = \begin{bmatrix} \frac{\lambda_2(1-\nu^2)}{E(\lambda_1\lambda_2-\nu^2)} & \frac{-\nu(1-\nu^2)}{E(\lambda_1\lambda_2-\nu^2)} & 0 \\ \frac{-\nu(1-\nu^2)}{E(\lambda_1\lambda_2-\nu^2)} & \frac{\lambda_1(1-\nu^2)}{E(\lambda_1\lambda_2-\nu^2)} & 0 \\ 0 & 0 & 1/G \end{bmatrix} \begin{Bmatrix} \bar{\sigma}_x \\ \bar{\sigma}_y \\ \bar{\tau}_{xy} \end{Bmatrix} \quad (h)$$

From assumption (2) and equations (b) and (h) we can obtain the actual stress in the plate and ribs.

$$\begin{Bmatrix} \sigma_x \\ \sigma_y \\ \tau_{xy} \\ \sigma_1 \\ \sigma_2 \end{Bmatrix} = \begin{bmatrix} \frac{\lambda_2 - \nu^2}{(\lambda_1\lambda_2 - \nu^2)} & \frac{\nu(\lambda_1 - 1)}{(\lambda_1\lambda_2 - \nu^2)} & 0 \\ \frac{\nu(\lambda_2 - 1)}{(\lambda_1\lambda_2 - \nu^2)} & \frac{\lambda_1 - \nu^2}{(\lambda_1\lambda_2 - \nu^2)} & 0 \\ 0 & 0 & 1 \\ \frac{\lambda_2(1-\nu^2)}{(\lambda_1\lambda_2 - \nu^2)} & \frac{-\nu(1-\nu^2)}{(\lambda_1\lambda_2 - \nu^2)} & 0 \\ \frac{-\nu(1-\nu^2)}{(\lambda_1\lambda_2 - \nu^2)} & \frac{\lambda_1(1-\nu^2)}{(\lambda_1\lambda_2 - \nu^2)} & 0 \end{bmatrix} \begin{Bmatrix} \bar{\sigma}_x \\ \bar{\sigma}_y \\ \bar{\tau}_{xy} \end{Bmatrix} \quad (i)$$